Received: 9 December 2020 | Revised: 12 July 2021 | Accepted: 25 March 2022 | Published on: 4 May 2022

DOI: 10.1002/qj.4287

Quarterly Journal of the Royal Meteorological Society RMetS

RESEARCH ARTICLE

The impact of the QBO on the region of the tropical tropopause in QBOi models: Present-day simulations

F. Serva[1] | J. A. Anstey[2] | A. C. Bushell[3] | N. Butchart[4] | C. Cagnazzo[1,5] | L. J. Gray[6,7] | Y. Kawatani[8] | S. M. Osprey[6,7] | J. H. Richter[9] | I. R. Simpson[9]

[1]Institute of Marine Sciences, National Research Council, Rome, Italy

[2]Canadian Centre for Climate Modelling and Analysis (CCCma), Victoria, British Columbia, Canada

[3]Met Office, Exeter, UK

[4]Met Office Hadley Centre, Exeter, UK

[5]European Centre for Medium-Range Weather Forecasts (ECMWF), Reading, UK

[6]Atmospheric, Oceanic and Planetary Physics, University of Oxford, Oxford, UK

[7]National Centre for Atmospheric Science (NCAS), Oxford, UK

[8]Japan Agency for Marine-Earth Science and Technology (JAMSTEC), Yokohama, Japan

[9]National Center for Atmospheric Research (NCAR), Boulder, Colorado, USA

Correspondence
F. Serva, Institute of Marine Sciences, National Research Council, Rome, Italy.
Email: federico.serva@artov.ismar.cnr.it

Funding information
Environmental Restoration and Conservation Agency, Grant/Award Number: JPMEERF20192004; European Commission, Grant/Award Number: Copernicus Climate Change Service; Japan Society for the Promotion of Science, Grant/Award Number: JP18H01286, JP19H05702, JP20H01973; Met Office, Grant/Award Number: Hadley Centre Climate Programme; National Center for Atmospheric Research; National Science Foundation, Grant/Award Number: IA 1844590; Natural Environment Research Council, Grant/Award Number: NE/N018001/1; NE/P006779/1

Abstract

The processes occurring in the tropical tropopause layer (TTL) are of great importance for stratosphere–troposphere exchanges and the variability of the Earth's climate. Previous studies demonstrated the increasing ability of atmospheric general circulation models (AGCMs) in simulating the TTL, depending on factors such as the horizontal and vertical resolution, with the major role for physical parametrizations. In this work we assess the mean state and variability of the tropical upper troposphere and lower stratosphere simulated by 13 AGCMs of the Stratosphere–troposphere Processes And their Role in Climate Quasi-Biennial Oscillation initiative (QBOi) for the historical period. As these models internally generate quasi-biennial oscillations (QBOs) of the stratospheric zonal wind, we can analyse the simulated QBO influence on the TTL on interannual time-scales. We find that model biases in temperature near the tropopause are strongly related to water vapour concentrations in the lower stratosphere. A source of intermodel spread derives from stratospheric aerosols, as the responses to eruptions differ between those models prescribing volcanic aerosol forcing. The QBO influence on the thermal structure is generally realistic in the equatorial region, but the subtropical response is weak compared with the reanalysis. This is associated with a limited downward penetration of QBO winds, generally smaller QBO meridional widths, and weaker temperature anomalies, which disappear above the tropopause for most models. We discuss the QBO impacts on tropopause pressure and precipitation, characterized by large uncertainties due to the small signal in the observational records and sampling uncertainty. Realistic QBO connection with the troposphere in some models suggests that the underlying physical processes can be correctly simulated. Overall, we find that the QBOi models have limited ability to reproduce the observed modulation of the TTL processes, which is consistent with biases in the vertical and latitudinal extent of the simulated QBOs degrading this connection.

KEYWORDS

internal variability, quasi-biennial oscillation, stratosphere–troposphere coupling, tropical tropopause layer

1 | INTRODUCTION

The atmospheric properties near the tropical tropopause are influenced by a number of dynamical and chemical processes on different temporal and spatial scales (Fueglistaler *et al.*, 2009). Ranging from fast deep convection (e.g., Schoeberl *et al.*, 2018) to long-term trends related to changing atmospheric composition (e.g., Gettelman *et al.*, 2010), a wide range of phenomena determine the conditions of the tropical tropopause layer (TTL). This atmospheric region, found between 150 and 70 hPa (14 and 20 km), represents the transition between the turbulent troposphere and the stably stratified stratosphere (Randel and Jensen, 2013).

On interannual time-scales, the stratospheric quasi-biennial oscillation (QBO) of the equatorial zonal wind induces changes in the thermal structure and stratosphere–troposphere exchanges (Baldwin *et al.*, 2001). The alternation of westerly and easterly zonal wind shear zones is respectively associated with warm anomalies and cold anomalies in the lower stratosphere (Plumb and Bell, 1982). By virtue of the thermal wind balance, anomalous upwelling and lower temperatures characterize the equatorial stratosphere during the easterly QBO phase (E), whereas a downwelling anomaly and higher temperatures are induced in the westerly phase (W). Although the QBO amplitude decays with latitude within the inner tropics, the equatorial changes induce thermal and residual circulation anomalies that extend beyond the tropical stratosphere to the Subtropics and can impact the surface (Gray *et al.*, 2018).

Focusing on the tropical region, the seasonal cycle is a major factor controlling temperature and water vapour fluctuations in the tropical upper troposphere and lower stratosphere (Rosenlof, 1995). On interannual time-scales, the QBO-induced anomalies reach the tropopause, modulating the amount of water vapour in the stratosphere (Giorgetta and Bengtsson, 1999; Tian *et al.*, 2019). At the same time, the QBO influences the distribution of tropical deep convective systems depending on the QBO phase (Collimore *et al.*, 2003; Liess and Geller, 2012), though the mechanisms behind this process are still a topic of research (Nie and Sobel, 2015). The anomalies related to El Niño-Southern Oscillation (ENSO) are relatively less important near the tropopause level (Randel and Wu, 2015).

In this article we analyse the simulations of the recent past performed with 13 atmospheric general circulation models (AGCMs) participating in the Quasi-Biennial Oscillation initiative (QBOi), a project aimed at assessing the ability of current models to simulate the QBO (Butchart *et al.*, 2018; Anstey *et al.*, 2020). We focus on the atmospheric response to westerly and easterly QBO phases, including the subtropical influence of the TTL processes. The QBOi models differ in many aspects, but all except one employ parametrization of non-orographic gravity waves (NOGWs), in some cases linked to their tropospheric sources (related to convection). Though the parametrized momentum forcing allows realistic QBO-like oscillations in all the models, most of these are meridionally too narrow and too weak in the lower stratosphere compared with observations (Bushell *et al.*, 2020). We discuss the implications of these biases and how model shortcomings in simulating the QBO can alter its modelled influence on the tropical climate system. To our knowledge, these topics have not been considered in detail in previous modelling studies, possibly due to the lack of QBO-resolving model ensembles, which are now increasingly available (e.g., Richter *et al.*, 2020).

2 | DATA AND METHODS

In order to assess how the QBOi models simulate the observed upper troposphere and lower stratosphere variability, we consider the Experiment 1 (Exp1) outputs of 13 AGCMs, which contributed up to three realizations to the QBOi archive, covering approximately the period 1979–2008. Further details on the models[1] are given in Table 1. In the Exp1 protocol, sea surface temperatures (SSTs) and sea ice are prescribed following observations, and time-varying forcings (greenhouse gases, solar radiation) are included. The formulation for ozone concentrations and aerosols depend on the model configuration and the experiment protocol left some freedom for modelling groups to choose these—more details can be found in Butchart *et al.* (2018). Some basic characteristics of these models relevant for this work are reported in Table 1. In particular, we report the approximate vertical resolution in the TTL region, which is key for the representation of wave activities (Fujiwara *et al.*, 2012; Holt *et al.*, 2020).

As in other QBOi studies on Exp1, we use as reference the ERA-Interim reanalysis (Dee *et al.*, 2011), produced by the European Centre for Medium Range Weather Forecasts (ECMWF). The representation of the TTL in ERA-Interim is comparable with that of other recent reanalyses (Tegtmeier *et al.*, 2020; Wang *et al.*, 2020). The reanalysis forecast model has 60 levels (https://www.ecmwf.int/en/forecasts/documentation-

[1]Note that here we consider realization r2i1p1 of the ECHAM5sh model, as r1i1p1 used in previous studies is affected by an error in the oceanic boundary conditions, which has now been fixed. For the current analyses, differences between the two realizations are relatively small (not shown).

TABLE 1 The QBOi models analyzed in this study and some of their characteristics

Model	Period (realiz.)	Horiz. res.	Vert. lev.	dz [m]	NOGW	Convection
60LCAM5	1975–2012 (2)	100 km	60	500	Lindzen (1981) Richter *et al.* (2010)	Zhang and McFarlane (1995)
AGCM-CMAM	1979–2009 (3)	281 km	113	500	Scinocca (2003)	Zhang and McFarlane (1995)
ECHAM5sh	1979–2008 (1)	210 km	95	650	Serva *et al.* (2018)	Tiedtke (1989) Nordeng (1994)
EMAC	1979–2012 (1)	310 km	90	650	Hines (1997)	Tiedtke (1989)
HadGEM2-A	1979–2006 (1)	1.875° × 1.25°	60	1150	Warner and McIntyre (1999)	Gregory and Rowntree (1990)
HadGEM2-AC	1979–2006 (1)	1.875° × 1.25°	60	1150	Warner and McIntyre (1999) Choi and Chun (2011)	Gregory and Rowntree (1990)
LMDz6	1979–2008 (1)	2.5° × 1.25°	79	1050	Lott *et al.* (2012) Lott and Guez (2013) de la Cámara and Lott (2015)	Hourdin *et al.* (2013)
MIROC-AGCM-LL	1979–2009 (3)	125 km	72	550	None	Emori *et al.* (2001)
MIROC-ESM	1979–2008 (3)	310 km	80	750	Hines (1997)	Emori *et al.* (2001)
MRI-ESM 2.0	1979–2009 (1)	83 km	80	500	Hines (1997)	Yoshimura *et al.* (2015)
UMGA7	1979–2008 (3)	1.875° × 1.25°	85	700	Warner and McIntyre (1999)	Gregory and Rowntree (1990)
UMGA7gws	1979–2008 (3)	1.875° × 1.25°	85	700	Warner and McIntyre (1999) Bushell *et al.* (2015)	Gregory and Rowntree (1990)
WACCM5-110L	1979–2012 (3)	1.25° × 0.94°	110	450	Lindzen (1981) Richter *et al.* (2010)	Zhang and McFarlane (1995)

Note: The horizontal resolution at the equator is reported either in kilometres or in longitude–latitude degrees, and the number of vertical levels is given in the fourth column. The approximate vertical resolutions (dz) in the tropical tropopause layer (15–20 km) are from Butchart *et al.* (2018, figure 5). See the text for more details. NOGWs: non-orographic gravity waves.

and-support/60-model-levels; last accessed November 2020) and an approximate resolution of 900 m in the TTL. Data on the same pressure levels specified by the QBOi protocol are considered, with a rather coarse resolution (∼20 hPa) in the tropopause layer.

Table 1 also lists the schemes used to parametrize NOGWs and convection. Parametrization of NOGW drag has proven fundamental for driving realistic QBOs in AGCMs (Giorgetta *et al.*, 2002; Scaife *et al.*, 2000). Spectral schemes such as those of Warner and McIntyre (1999) and Hines (1997) are used, with a stochastic modification in ECHAM5sh, whereas 60LCAM5, WACCM-110L, HadGEM2-AC, LMDz6, and UMGA7gws link the NOGW spectrum to convective activity, either through total precipitation or parameters from the cumulus scheme. Only MIROC-AGCM-LL is able to produce a QBO without an NOGW parametrization. The parametrized convection (rightmost column in Table 1) is very important for the simulation of atmospheric waves driving the QBO (e.g., Takahashi, 1996). For cumulus convection, different schemes are used by the QBOi models, influencing both precipitation and the tropical wave spectrum (Holt *et al.*, 2020; Horinouchi *et al.*, 2003). One frequent bias is represented by the too weak and frequent simulated precipitation (e.g., Dai, 2006). This has been explicitly addressed in MIROC-based models, by using a relative humidity method to improve the representation of convectively coupled and equatorially trapped waves (Kawatani *et al.*, 2009; 2010), and with a spectral cumulus scheme in MRI-ESM 2.0, which improved the simulation of organized convection (Yoshimura *et al.*, 2015). Note that MRI-ESM 2.0 is an updated version of the model documented in Butchart *et al.* (2018), and it includes changes aimed at improving the modelled QBO (Yukimoto *et al.*, 2019).

For characterizing the QBO influences in the tropical climate, we analyse monthly mean variables, considering surface temperature, total precipitation, zonal wind, temperature, water vapour concentration, residual velocities and tropopause pressure. The meridional and upward residual winds are available in the QBOi archive, and are defined in the transformed Eulerian mean framework

(Andrews *et al.*, 1987, p. 128). For ERA-Interim, they are calculated as described in Serva *et al.* (2018). The tropopause pressure is not available from the QBOi archive, and it is calculated with the lapse-rate tropopause (LRT) method, which identifies the tropopause as the pressure level in the upper troposphere where the vertical temperature gradient ($-\partial T/\partial z$) falls below $2\,\mathrm{K\cdot km^{-1}}$. Two-sided finite differences are used to compute vertical gradients. We note that higher temporal and spatial resolution should be preferred for detailed analysis (Tegtmeier *et al.*, 2020).

Though multiple choices can be found in the literature for defining a QBO index (Huesmann and Hitchman, 2001), the zonal wind biases need to be carefully considered when dealing with model outputs. Westerly and easterly phases are identified from the zonal mean zonal wind at selected pressure levels, defining QBO phases when the index exceeds a given threshold value, using area averages between 5° latitude from the Equator. To study the impacts on tropospheric variables (tropopause pressure and precipitation), we employ deseasonalized quantities instead of raw values in order to isolate the interannual variability associated with the QBO.

When we need to isolate the influence of a process from a certain quantity, we do so by means of a (multiple) linear regression method; for example, see Mitchell *et al.* (2015). This allows the variability to be associated with a number of predictors x_i, so that the predictand y can be expressed as $y = \sum_i x_i \cdot c_i + R$, where c_i are regression coefficients and R is a residual term. All predictors are here considered at lag zero.

As ancillary data, we use the monthly averages of the solar flux at 10.7 cm as a proxy for solar activity (Tapping, 2013) and the aerosol optical depth (AOD) in the Tropics (Hansen *et al.*, 1996). Peaks in stratospheric AOD within 15° from the Equator are used to identify the year and month when volcanic aerosol loadings are maximized, and these are used as eruption dates for the composites.

3 | RESULTS AND DISCUSSION

The application to seasonal prediction ensures a broad interest in how multiseasonal variability in the stratosphere propagates downwards, first into the region of the TTL and ultimately into the troposphere. Hence, we start the assessment of the TTL of the QBOi models in Exp1 by considering some basic diagnostics for the lower stratospheric temperature and water vapour in Section 3.1. As a dominant mode of variability in the tropical stratosphere which is represented by all the models in QBOi Exp1, the QBO is an obvious candidate for introducing interannual variability into the TTL region, an impact explored in Section 3.2. Subsequent QBO impacts on the tropopause and lower troposphere are then evaluated in Section 3.3.

3.1 | Climatological features and interannual variability in the tropical stratosphere

The temperature seasonal cycle near the tropical tropopause is a well-known diagnostic used to characterize the TTL conditions in models (Gettelman *et al.*, 2010). In Figure 1a we show the averaged temperature in the tropical region at the 100 hPa pressure level, as a function of the calendar month. We average area-weighted zonal mean temperatures within ±10° latitude from the Equator. From Figure 1a we can see how the multimodel mean agrees better with ERA-Interim than most individual models, due to cancellation of model errors. While the two variations of the HadGEM model have a warm bias (up to 4 K), the two ECHAM-based models (ECHAM5sh and EMAC) are colder year-round (of the order of 2 K) compared with the reanalysis. It is worth noting that the warm bias observed for the HadGEM models has been corrected in UM-based models thanks to model developments related to numerical and microphysical aspects (Hardiman *et al.*, 2015). Also the sensitivity to ozone distribution in the TTL (Oh *et al.*, 2018) can potentially lead to some differences, affecting the annual cycle properties as well (Ming *et al.*, 2017), but we expect these to be minor—see Butchart *et al.* (2018, figure 6b). Only MRI-ESM 2.0 has interactive ozone, whereas other models employ a seasonally varying distribution that includes the long-term solar and stratospheric chlorine variability. The role of the ozone QBO is therefore neglected, although this can contribute substantially to the QBO signal in temperature (Butchart *et al.*, 2003; Li *et al.*, 1995). Seasonal variation of the upwelling strength determines a marked seasonal cycle in the tropopause temperature (Rosenlof, 1995). The maximum annual temperatures (195 K in the reanalysis) occur in the boreal summer, whereas the minimum temperatures are found near to the boreal winter solstice. The observed annual cycle (e.g., Randel *et al.*, 2000) is well reproduced in most cases, but ECHAM-based models show less pronounced seasonal variation, possibly due to an overly small upwelling seasonality (Abalos *et al.*, 2012).

The seasonal cycle of tropopause temperature determines the variable efficacy of the cold trap, which is key for the freeze-drying process modulating the amount of water vapour reaching the lower stratosphere (Fueglistaler *et al.*, 2009). To quantify this relationship, we consider the water vapour concentration at 85 hPa, again averaged

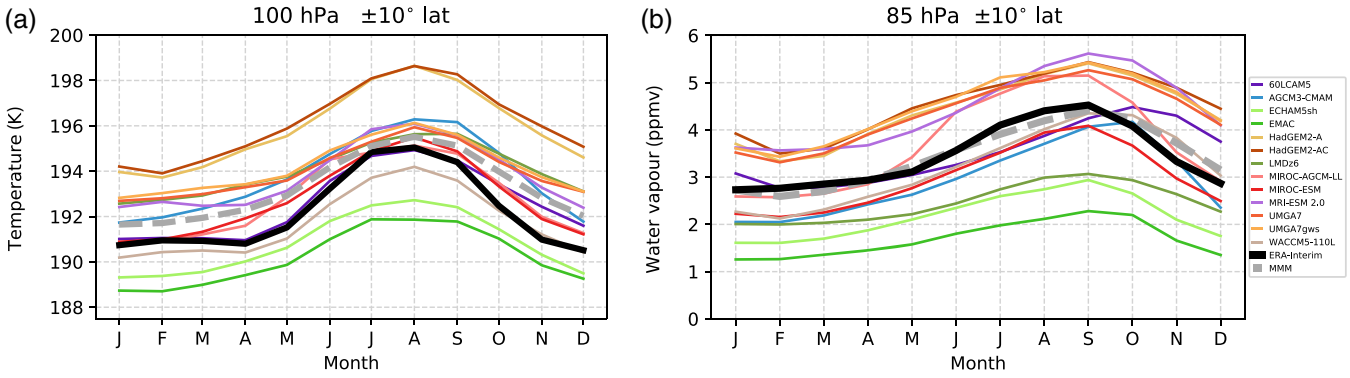

FIGURE 1 Seasonal cycle of (a) the temperature at 100 hPa and (b) water vapour at 85 hPa, averaged in the equatorial region (10° from the Equator). ERA-Interim is indicated with the thick black line, and the multimodel mean with the dashed grey line [Colour figure can be viewed at wileyonlinelibrary.com]

within 10° from the Equator. Whereas the water vapour cycle lags that of temperature by 1 month (maxima occurring around September and August, respectively), the results shown in Figure 1b are somewhat more complex. As expected, model temperature biases are reflected by those in water vapour concentrations, with colder models (EMAC, ECHAM5sh) being drier and with warmer models (HadGEM2-A and HadGEM2-AC) being moister. However, some models, like MRI-ESM 2.0, which are not outliers in temperature, are outstanding for their high water vapour concentrations in the second half of the calendar year.

Multiple processes contribute to the interannual variability of near-tropopause temperatures, including external forcings such as changes in solar radiation (Gray *et al.*, 2010) and stratospheric aerosols (Robock, 2004). The temperature anomalies, computed as the departure from the seasonal cycle for the common reference period 1980–2005, are shown in Figure 2a. Substantial interannual variability can be seen, due to the superposition of factors like the ENSO, the QBO, and long-term changes. The fluctuations have a typical amplitude of 1–2 K, but in some models (such as MRI-ESM 2.0 and MIROC-AGCM-LL) there are notable positive anomalies (3–5 K) in the early 1980s and 1990s. This coincides with the occurrence of major volcanic eruptions, namely those of El Chichón (Mexico 1982) and Pinatubo (Philippines 1991), marked by red triangles in Figure 2. The prominence of the latter temperature peak is consistent with the greater amounts of volcanic aerosols injected into the atmosphere. Also note that, in ERA-Interim, whereas the volcanic aerosol loadings do not vary interannually, the assimilation of upper atmospheric observations help to reproduce the observed patterns (e.g., Fujiwara *et al.*, 2015). The water vapour anomalies around the time of the eruptions are shown in Figure 2b,c for the 1982 and 1991 events. Positive anomalies are evident for MIROC-AGCM-LL and MRI-ESM 2.0 for both cases, with larger moistening for the Pinatubo eruption, also seen in HadGEM and 60LCAM5 models during 1992. The anomalies after major eruptions merit more detailed investigation because, although the impact of each is transient, they represent a systematic additional forcing for the climatologies of temperature and water vapour in those models that represent them explicitly, which for some models shifts their humidity values to the upper range of the QBOi ensemble for several months after the eruption dates. Such impacts can be quantified for Exp1.

By looking at the temporal evolution of lower stratospheric temperatures (not shown), we have identified seven QBOi models that included time-varying stratospheric aerosols (they were not specified in the protocol). Since the anomalies due to volcanic aerosols could also be masked by other factors, such as the QBO (Angell, 1997), then in order to isolate the volcanic aerosol effects we remove the influence of a series of patterns by multiple linear regression. Starting from deseasonalized zonal mean temperatures, we subtract the variability associated with the ENSO index for the 3.4 region, the QBO (with two indices for the zonal mean zonal wind at 20 and 50 hPa), a linear trend, and total solar irradiance. Different approaches have been used in the literature (e.g., different lags or additional predictors can be considered), leading to some differences in the results. The results of this methodology based on Mitchell *et al.* (2015) and applied to ERA-Interim data are in good agreement with previous reanalysis studies (Fujiwara *et al.*, 2015). The volcanic anomalies are identified as the residual of the multiple linear regression, averaged over the 12 months following the month of the AOD peak, minus the average of the three preceding years. Differences are deemed significant when they exceed two standard deviations of yearly mean values.

The results for El Chichón and Pinatubo are reported in Figure 3 and 4, respectively. It is clear how the

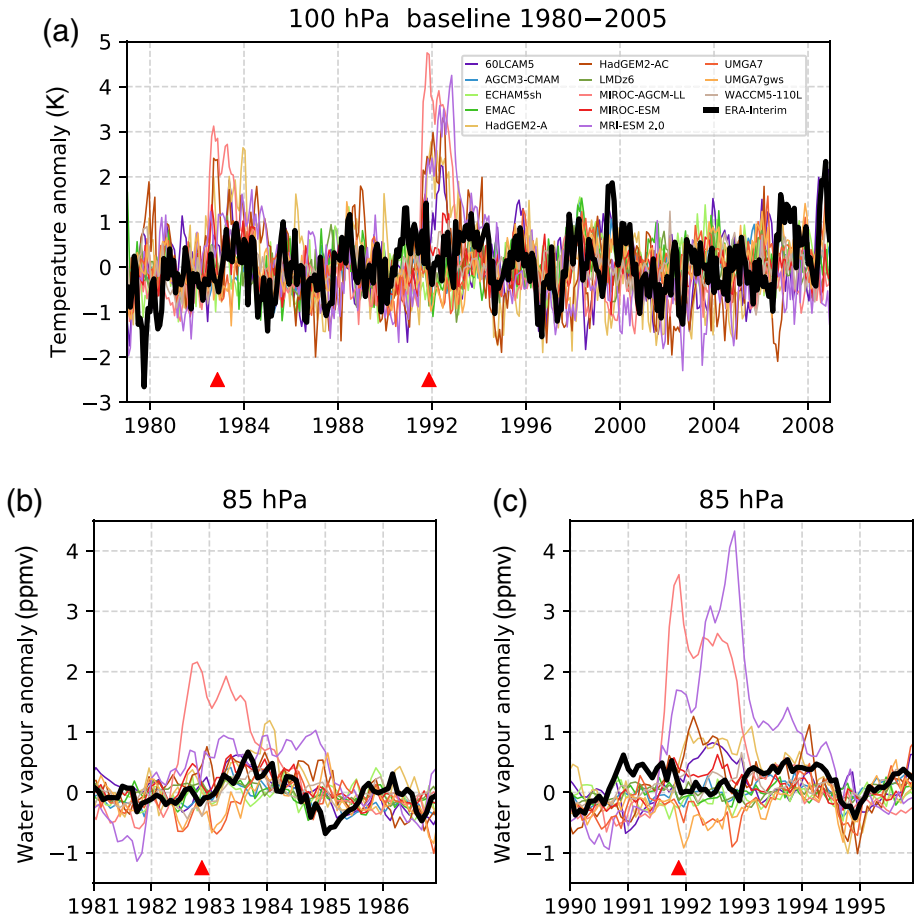

FIGURE 2 Time series of the monthly mean deseasonalized (a) temperature anomaly at 100 hPa and (b, c) water vapour at 85 hPa, averaged within 10° from the Equator. Anomalies are computed as departures from the period 1980–2005; results for multiple ensemble members are averaged. Water vapour anomalies are shown near the eruption dates, marked by red triangles (see text for details) [Colour figure can be viewed at wileyonlinelibrary.com]

modelled temperature anomalies are positive in the TTL after the latter eruption; and given the geographical location of the two volcanoes, the Pinatubo anomalies are more centred near the Equator. The spread between models in representing the same eruption is quite substantial, which may depend on the prescription of volcanic aerosols (e.g., Löffler *et al.*, 2016), but also on the phase of the QBO at the time of the eruption. Warming tends to be maximized at about 100 hPa in the TTL, but the warmed layer is shallower in MIROC-AGCM-LL and MRI-ESM 2.0, two of the models showing larger anomalies in Figure 2a. Tropospheric anomalies are small for both the reanalysis and models in the two cases. The TTL warming pattern is extended towards the Subtropics, more often in the Northern Hemisphere especially for the Pinatubo eruption, consistent with changes in the residual circulation (Toohey *et al.*, 2014). The extratropical response is underestimated by most models (not shown), likely due to sampling variability, but the observed response is uncertain given the very small number of events available in the record.

Summarizing, the TTL warming (3 K or more) due to the eruptions is seen in the models that prescribed volcanic aerosol forcing and would modulate the cold trap efficiency, affecting stratospheric water vapour concentrations (e.g., Soden *et al.*, 2002) and contributing to the spread of Figure 1. The magnitude of this effect is expected to vary between the QBOi models due to differences in the relative position and depth of the warmed layer with respect to the temperature minimum near the tropical tropopause.

3.2 | QBO zonal mean impacts in the TTL

Even in those models that represent volcanic forcings, the QBO impact on the TTL region is important because the QBO is accompanied by temperature anomalies at the Equator due to the thermal wind balance, inducing a compensating residual circulation in the Subtropics (Plumb and Bell, 1982). To get a general overview of the tropical stratosphere during opposite QBO phases, in Figure 5 we report the difference between westerly and easterly QBO conditions for zonal wind, temperature, and residual circulation $(\overline{v}^*, \overline{w}^*)$. Here, a month is assigned to a certain QBO phase when the zonal mean zonal wind at 50 hPa is westerly (W, above 1.5 $m \cdot s^{-1}$) or easterly (E, below $-1.5\ m \cdot s^{-1}$). Note that the two phases are not symmetric in duration or amplitude (not shown). Though other pressure

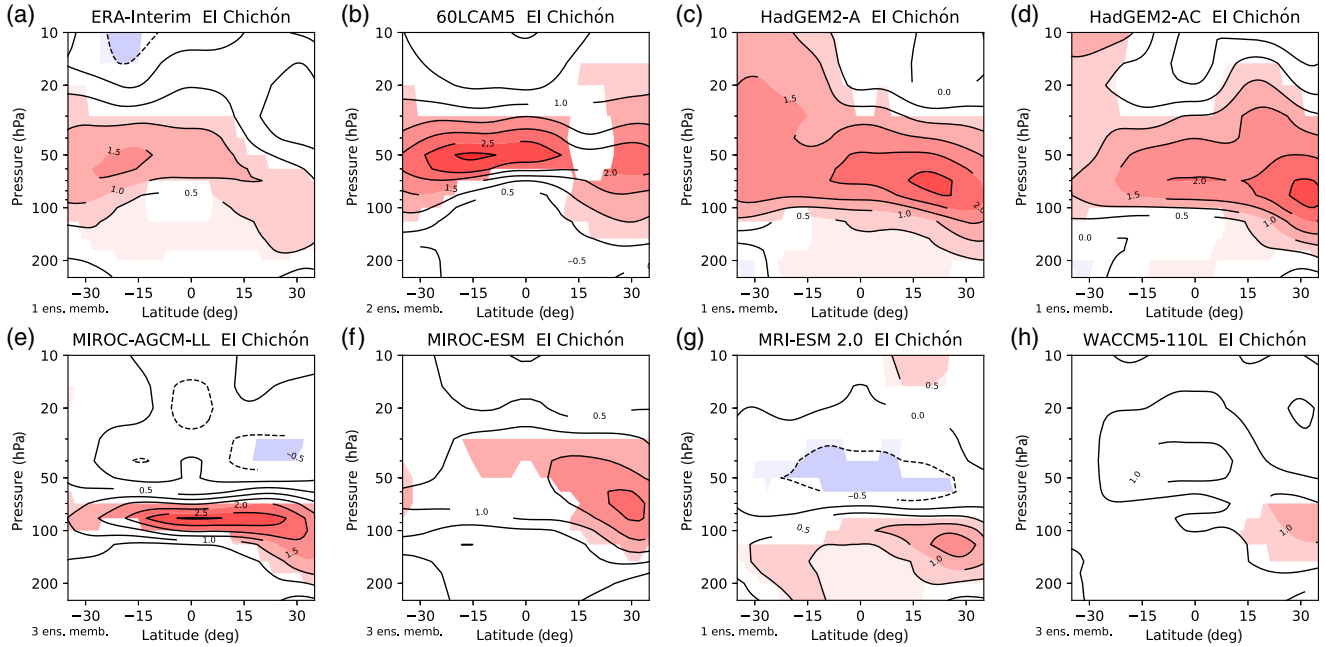

FIGURE 3 Residual temperature anomalies (K) calculated from the year following the 1982 El Chichón eruption minus the previous 3 years for (a) the ERA-Interim reanalysis and (b–h) the Exp1 model simulations that include volcanic aerosols. Anomalies exceeding ±2 standard deviations of the yearly mean values are shaded (red positive, blue negative). Results for multiple ensemble members (reported in the bottom left corner) are averaged [Colour figure can be viewed at wileyonlinelibrary.com]

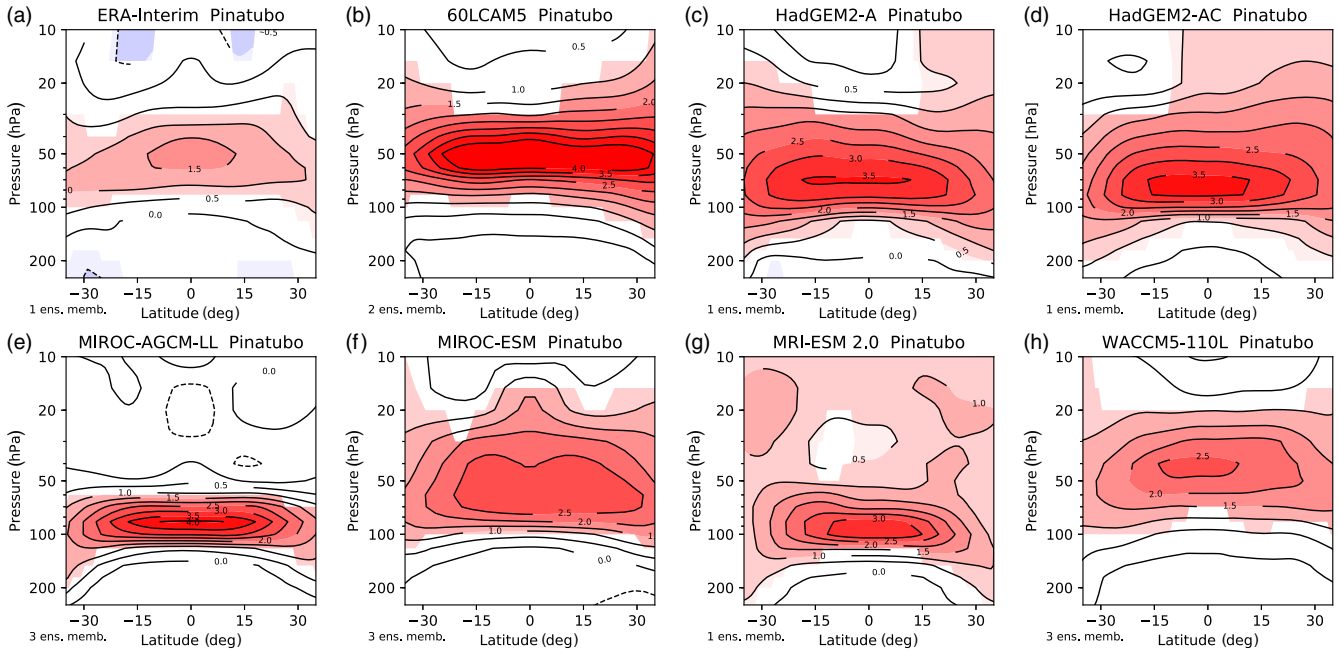

FIGURE 4 The same as Figure 3 but for the 1991 Pinatubo eruption [Colour figure can be viewed at wileyonlinelibrary.com]

levels could be selected, 50 hPa is frequently used to define the QBO, and the chosen thresholds allow us to obtain a reasonable sample size and to highlight relevant features.

For the zonal wind (lines in Figure 5) the largest anomalies are found near the 10 hPa and the 50 hPa levels in both the reanalysis and models, but the pattern is fairly different among models in the lower stratosphere and off-Equator. For most models (especially LMDz6, MIROC-AGCM-LL and, MIROC-ESM) the differences near 50 hPa appear weaker and narrower in latitude.

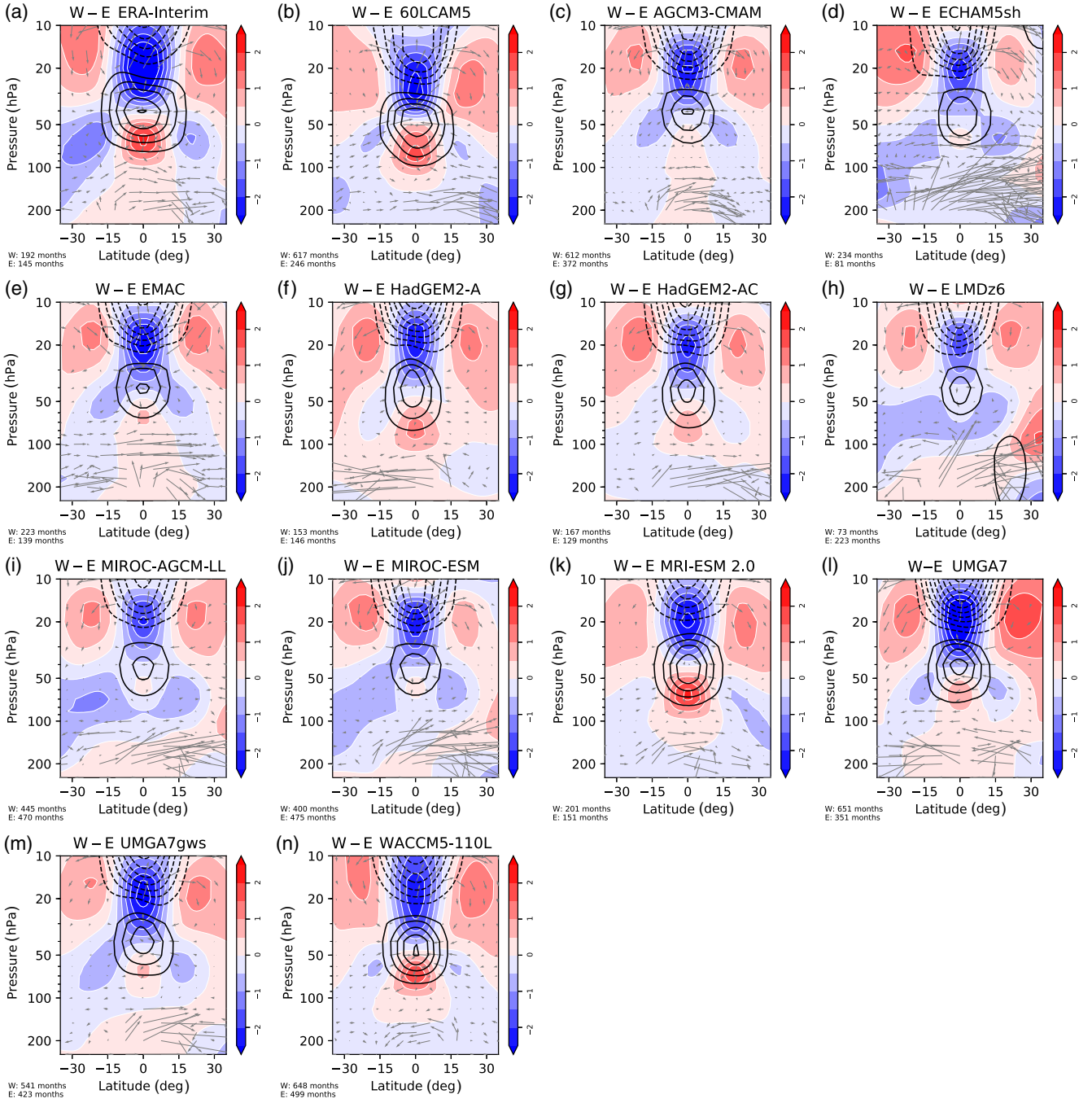

FIGURE 5 Composite zonal mean differences for the zonal mean zonal wind (units are $m \cdot s^{-1}$, black lines every $5\ m \cdot s^{-1}$, the zero contour is omitted), temperature (units are K, shadings), and residual circulation (grey arrows) for westerly (W) minus easterly (E) QBO conditions at 50 hPa. The vertical component of the residual circulation is multiplied by 220. The number of months used for compositing is indicated in the bottom left corner in each case [Colour figure can be viewed at wileyonlinelibrary.com]

Negative wind anomalies characterize the equatorial stratosphere above 25 hPa, owing to the vertical structure of the QBO. Overall, the QBOi models appear to have too weak wind amplitude in the lower stratosphere, as reported by (Bushell *et al.*, 2020).

The intermodel differences are substantial for the W – E composite of the zonal mean temperature (shadings in Figure 5), especially for the warm anomaly in the equatorial lower stratosphere, which is underestimated or even reversed in half of the models. The subtropical anomalies are also different from ERA-Interim, as cold anomalies do not extend to the subtropical upper troposphere in most models.

The non-local response to the QBO phases can be explained by virtue of the induced circulation anomalies (arrows in Figure 5). For the reanalysis (a), the region

of anomalous downwelling, which gives rise to adiabatic heating, is located below the maximum of the positive wind anomaly at the Equator (between 100 and 50 hPa), flanked in the Tropics by anomalous upwelling and cooling (roughly below 30 hPa, with an inverted V shape). Around 20 hPa, a cold anomaly is found at the Equator, with compensating downwelling and warm anomalies in the Subtropics. The models that do not reproduce the reanalysis pattern have a weaker, or even reversed, residual circulation anomaly, especially in the lower stratosphere (such as HadGEM2-A or LMDz6). Most of them underestimate the latitudinal width of the QBO-induced thermal anomalies, potentially disconnecting the phase of the equatorial QBO from subtropical atmospheric conditions (Garfinkel and Hartmann, 2011).

To further illustrate how the temperature response differs among the models and from ERA-Interim, we show in Figure 6a–c the vertical profiles of the temperature anomalies at the Equator and in the Subtropics, obtained from Figure 5. The temperature anomaly at the Equator (Figure 6b) is weaker in most models between 100 and 50 hPa, except for 60LCAM5 around 90 hPa. The temperature profiles also differ aloft, since the cold anomalies between 40 and 10 hPa are underestimated by the models. For the lower stratosphere, a linear relationship between the strength of the zonal wind anomalies at 50 hPa and temperature at 70 hPa can be inferred from the scatter plot shown in Figure 6d. The relation between temperature and residual circulation is somewhat weaker (Figure 6e); however, as mentioned, the models with stronger residual downwelling better reproduce the thermal anomalies found for ERA-Interim. In the Subtropics (Figure 6a,c) the intermodel spread is large below 50 hPa, and most models have weaker cold anomalies below this level (less so for MIROC-AGCM-LL in the Southern Hemisphere and MRI-ESM 2.0 and 60LCAM5 in the Northern Hemisphere). These results highlight the intermodel spread in the representation of the equatorial structure of the QBO and the induced subtropical circulations, the latter being generally weaker in the models than in the reanalysis. As described in the next section, these biases have implications for the simulated influence of the QBO on the tropical troposphere in the models.

3.3 | QBO impacts on tropopause pressure and precipitation patterns

From the W – E composites we have found that most models underestimate the lower stratospheric temperature anomalies due to the QBO at the Equator and in the Subtropics. Previous studies have found that there is a robust observed response to lower stratospheric winds of the tropopause height (e.g., Rieckh *et al.*, 2014) and a QBO signal in precipitation (e.g., Collimore *et al.*, 2003), the two variables being related (Davis *et al.*, 2014; Xian and Fu, 2015). To test how well these processes are reproduced by the models, we again consider W – E composited differences, now defining QBO phases on the basis of the 70 hPa zonal mean zonal wind, similar to the approach of Gray *et al.* (2018) for the analysis of precipitation. Deseasonalization was not performed by Gray *et al.* (2018), but here is required to account for the wind biases in the lower stratosphere; westerly and easterly phases are defined when the index is above 1 $m \cdot s^{-1}$ or below −1 $m \cdot s^{-1}$, respectively.

Results are stratified by season, since seasonal variations are substantial for both the tropopause pressure and precipitation. Seasonal averaging has the disadvantage of further reducing the sample size (e.g., a 30-year realization would give only 30 June–July–August averages) and, hence, the statistical robustness of the results, particularly for models providing a single realization. The effects of ENSO are subtracted from the raw precipitation and tropopause pressure fields by means of a linear regression. The patterns of the ENSO regression are in agreement with previous studies: For precipitation (Supporting information Figure S1), positive coefficients characterize the eastern Pacific, especially the Niño 3.4 region (5° N–5° S, 170°–120° W), whereas negative coefficients border South American Pacific coasts (Niño 1+2 area, 0°–10° S, 90°–80° W; e.g., Fasullo *et al.*, 2018); for tropopause pressures (Supporting information Figure S2), negative coefficients characterize the subtropical latitudes in the Pacific (Hatsushika and Yamazaki, 2001; Rieckh *et al.*, 2014) in the models, except for MIROC-AGCM-LL. Further investigation into the modelled response of precipitation and tropopause properties to ENSO is ongoing within QBOi, by considering outputs with higher vertical resolution up to the upper troposphere.

In Figure 7 we show the seasonal averages and W – E composites for the LRT pressure for ERA-Interim. Results for the cold-point tropopause method are qualitatively similar, as illustrated in Supporting information Figure S3. The vertical movement of the tropical tropopause is well captured, with larger tropopause pressures in boreal summer and lower in winter (Seidel *et al.*, 2001), even if the vertical resolution of the data is insufficient to capture fine-scale variations (Tegtmeier *et al.*, 2020). Some longitudinal variations are present, but they are likely underestimated in the inner Tropics. The W – E QBO differences are more evident in boreal spring and winter, and some longitudinal asymmetries are visible, with significant anomalies over the Maritime Continent and the eastern Pacific. This seasonal dependence may be explained by the fact that, in boreal summer, tropopause pressures are higher

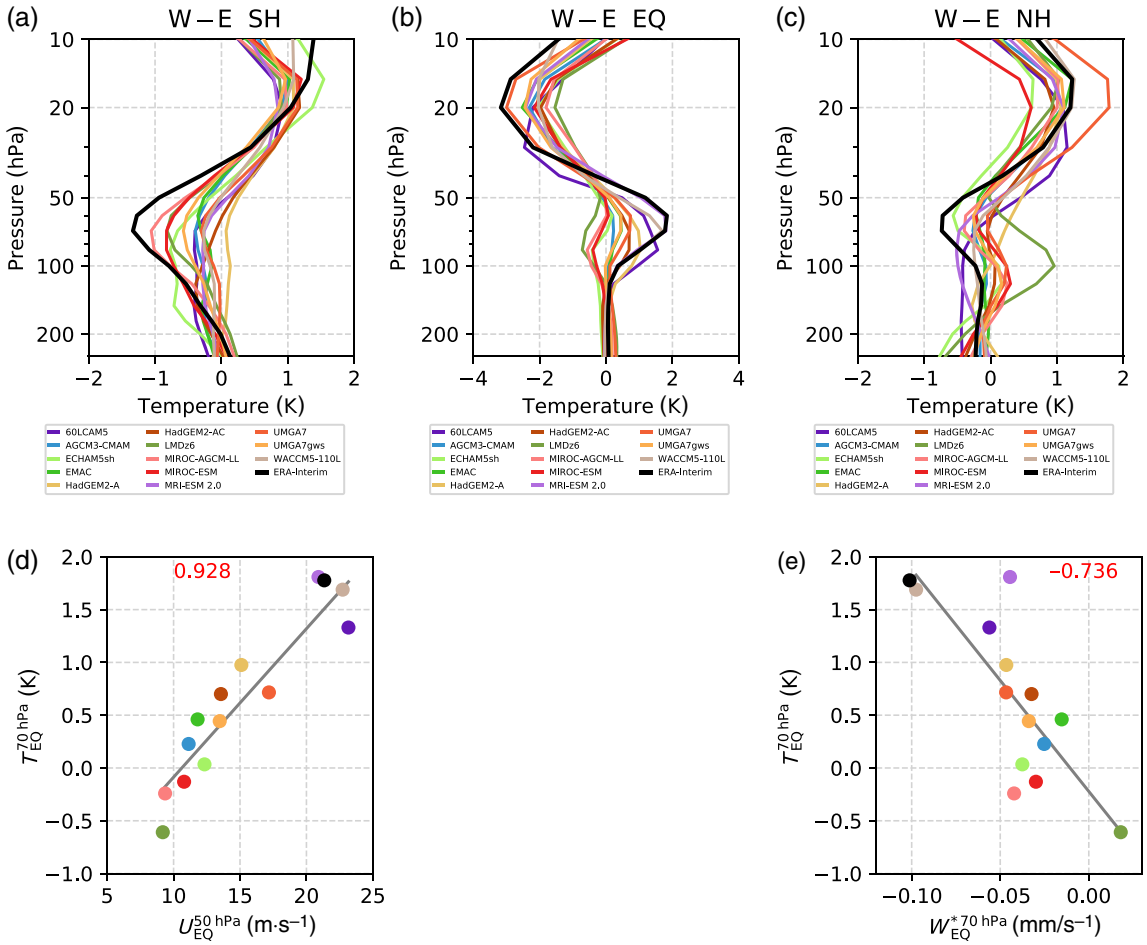

FIGURE 6 Mean profiles of temperature westerly (W) minus easterly (E) composites between latitudes (a) 20°–30° in the Southern Hemisphere (SH), (b) ±5° from the Equator (EQ), and (c) 20°–30° in the Northern Hemisphere (NH). Note the different range of the abscissa in (b). Scatter plots of the equatorial temperature composite difference at 70 hPa (d) against zonal wind at 50 hPa and (e) against vertical component of the residual circulation, as defined in (a)–(c). Regression lines for Quasi-Biennial Oscillation initiative models are shown in grey in (d) and (e), and the linear correlation coefficients (in red if $P < 0.05$) are given in the upper parts of (d) and (e) [Colour figure can be viewed at wileyonlinelibrary.com]

(and the tropopause at lower heights), farther from the influence of the lowermost QBO winds.

In Figure 8 we report the LRT pressure seasonal averages and W – E QBO composites from the QBOi models during December–January–February, for comparison with Figure 7a. The seasonal average spatial patterns are fairly different and unrealistic in some cases, with the tropopause pressures being lower (reaching up to 85 hPa) in EMAC and LMDz6. The longitudinal variations in the southern Subtropics (Luan *et al.*, 2020) are common to all models and ERA-Interim. Compared with ERA-Interim results, longitudinal asymmetries are more marked for most models. Significant positive differences at the Equator can be seen for 60LCAM5, WACCM-110L, UMGA7, and UMGA7gws, whereas more confined or weaker positive anomalies are found in AGCM3-CMAM, ECHAM5sh, the two HadGEM models, MIROC-ESM, and MRI-ESM 2.0, with large intermodel differences. The signal is pronounced in 60LCAM5 and more zonal than that observed, including over the western Pacific. The anomalies are even reversed in MIROC-AGCM-LL, also using other indices to define the lower stratospheric QBO (not shown), possibly due to its small QBO amplitude in the lower stratosphere (Bushell *et al.*, 2020).

To better illustrate the longitudinal characteristics of the W – E differences (Tegtmeier *et al.*, 2020a), in Figure 9 we show scatter plots of the tropopause pressure anomalies as a function of the QBO amplitude at 70 hPa. For simplicity, the amplitude is defined as the range of the deseasonalized QBO index (i.e., $U_{EQ}^{range} = U_{EQ}^{max} - U_{EQ}^{min}$). We consider spatially averaged anomalies over three regions: the Maritime Continent (MC, 10° N–10° S, 80°–150° E), tropical Africa (TA, 10° N–10° S, 5°–45° E), and eastern Pacific–South America (ES, 10° N–10° S, 100°–40°

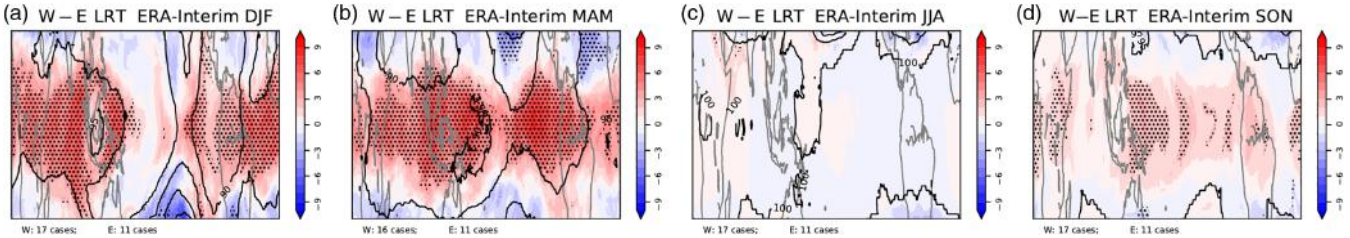

FIGURE 7 Longitude–latitude maps of mean tropopause pressure (solid lines) and westerly (W) minus easterly (E) differences (shadings) for ERA-Interim, using the lapse rate definition for the December–January–February (DJF), March–April–May (MAM), June–July–August (JJA), and September–October–November (SON) seasons. Units are hPa. Differences significant at the 95% confidence level according to a two-sided *t*-test are dotted. Positive anomalies indicate that the tropopause is located at lower altitudes, and vice versa. The number of seasons considered is reported at the bottom. LRT: lapse-rate tropopause [Colour figure can be viewed at wileyonlinelibrary.com]

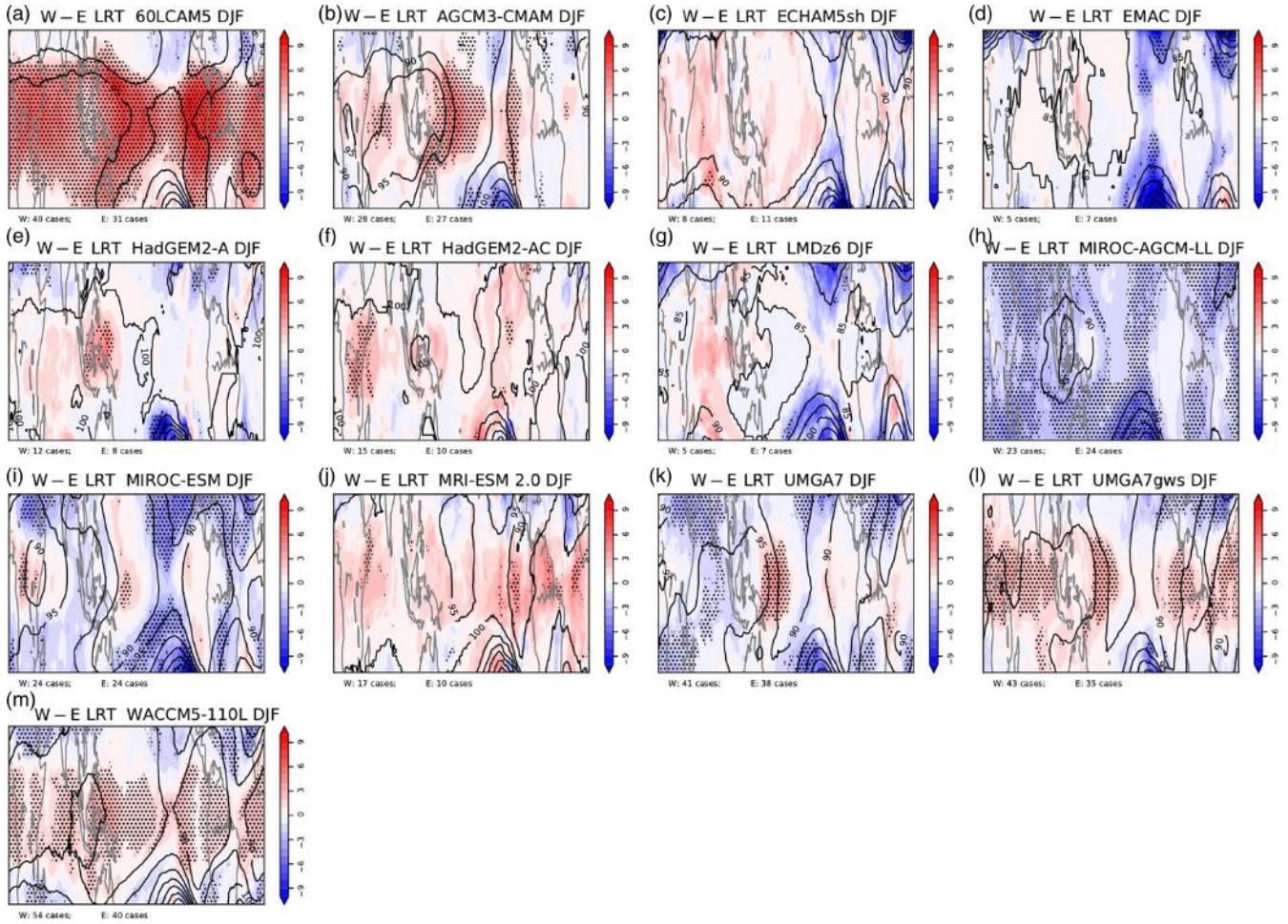

FIGURE 8 The same as Figure 7 but for the Exp1 models in the December–January–February (DJF) season. LRT: lapse-rate tropopause [Colour figure can be viewed at wileyonlinelibrary.com]

W) regions, shown in red in Figure S5. With the exception of 60LCAM5, WACCM5-110L, and MRI-ESM 2.0, the estimated QBO amplitude at 70 hPa is smaller than the reanalysis, and for most models the sign of the anomalies is consistent with that observed. As seen in the longitude–latitude maps (Figure 8), there are, however, models with realistic QBO amplitudes, but negative W – E differences. The slope of the regression line for the models is positive in all the three regions, indicating that the amplitude of the QBO in the lower stratosphere is correlated with the response of the tropopause pressure. Further analysis is required to better understand the reasons for the

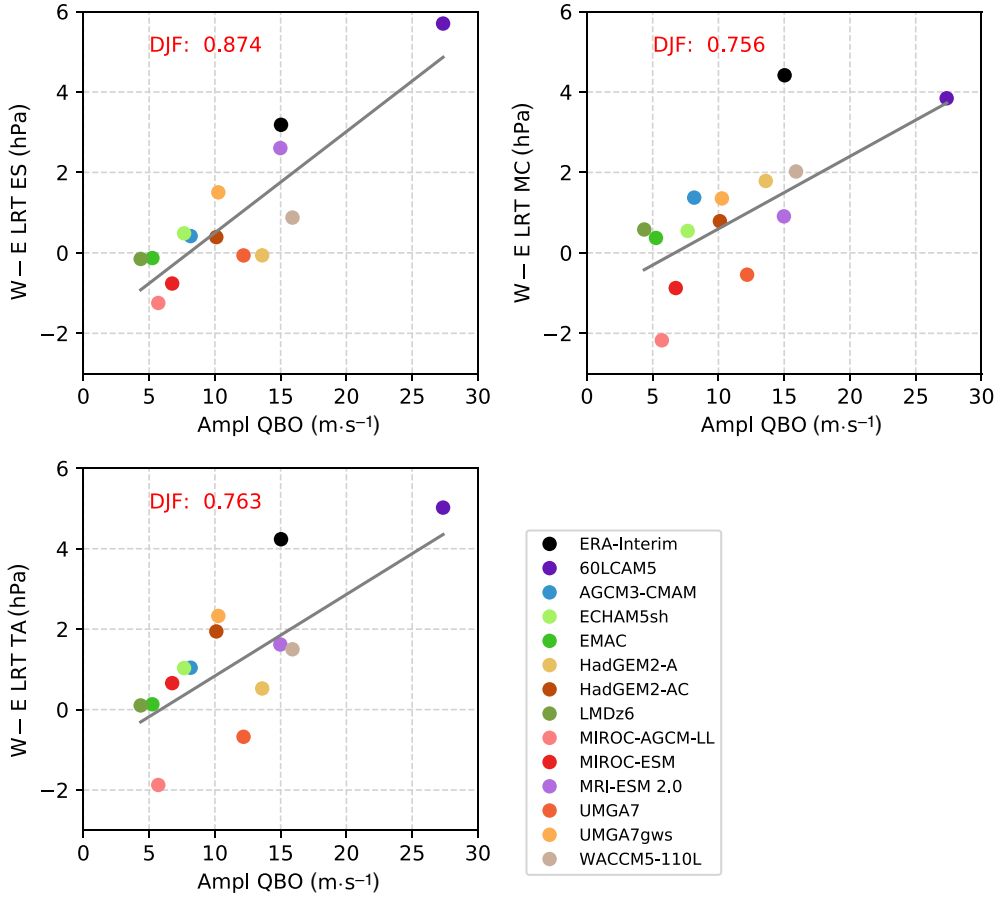

FIGURE 9 Scatter plots for the westerly (W) minus easterly (E) tropopause pressure anomalies against the amplitude of the lower stratospheric quasi-biennial oscillation (Ampl QBO) index in December–January–February (DJF) for three selected regions: eastern Pacific–South America (ES), Maritime Continent (MC), and tropical Africa (TA); see text and Supporting information for details. Regression lines for the Quasi-Biennial Oscillation initiative models are reported in grey, together with the linear correlation coefficients (in red if $P < 0.05$) in the upper part of the plots. Note that the variable on the abscissa is the same in the three plots. LRT: lapse-rate tropopause [Colour figure can be viewed at wileyonlinelibrary.com]

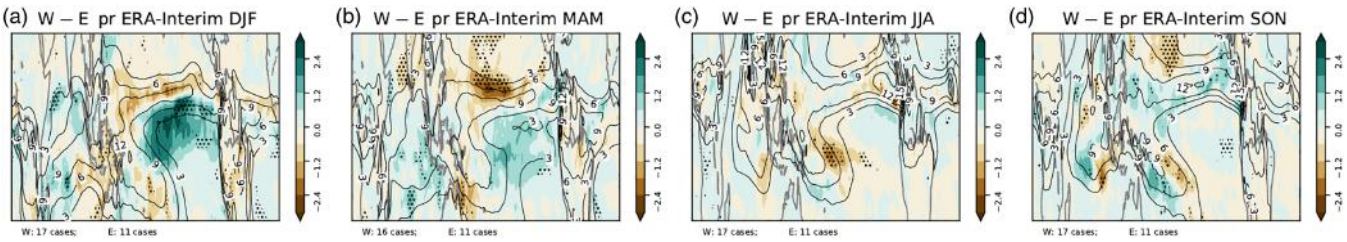

FIGURE 10 Longitude–latitude maps of mean total precipitation (pr, solid lines) and (W) minus easterly (E) differences (shadings) for ERA-Interim, for the December–January–February (DJF), March–April–May (MAM), June–July–August (JJA), and September–October–November (SON) seasons. Units are mm·day^{-1}. Differences significant at the 95% confidence level according to a two-sided t-test are dotted. The number of seasons considered is reported at the bottom [Colour figure can be viewed at wileyonlinelibrary.com]

negative anomalies shown by some models, as we cannot exclude effects due to the diagnostic procedure.

Following the methodology used for the tropopause pressure, we consider how the models represent the QBO influence on tropical precipitation. This relationship has been previously documented (Collimore *et al.*, 2003; Gray *et al.*, 2018; Liess and Geller, 2012; Nie and Sobel, 2015), and it is believed to involve the effect of wind shear on convection, tropopause height, and stability, but the underlying mechanisms are not well known. This effect is particularly evident over the Pacific, where the QBO may modulate the local Hadley circulation, and the effects of ENSO are substantial (here, these are removed by linear regression). We note that the observed precipitation response to the QBO is still an active topic of research; and due to the short observational record and internal variability, it is challenging to validate this process in the models.

In Figure 10, the mean total precipitation and composite W − E differences for ERA-Interim are shown. Given the low signal-to-noise ratio of this variable, seasonal or even annual means are useful to obtain a clearer picture (Gray *et al.*, 2018). Seasonal variability, including the northward shift of the intertropical convergence zone (ITCZ) and precipitation associated with the Asian

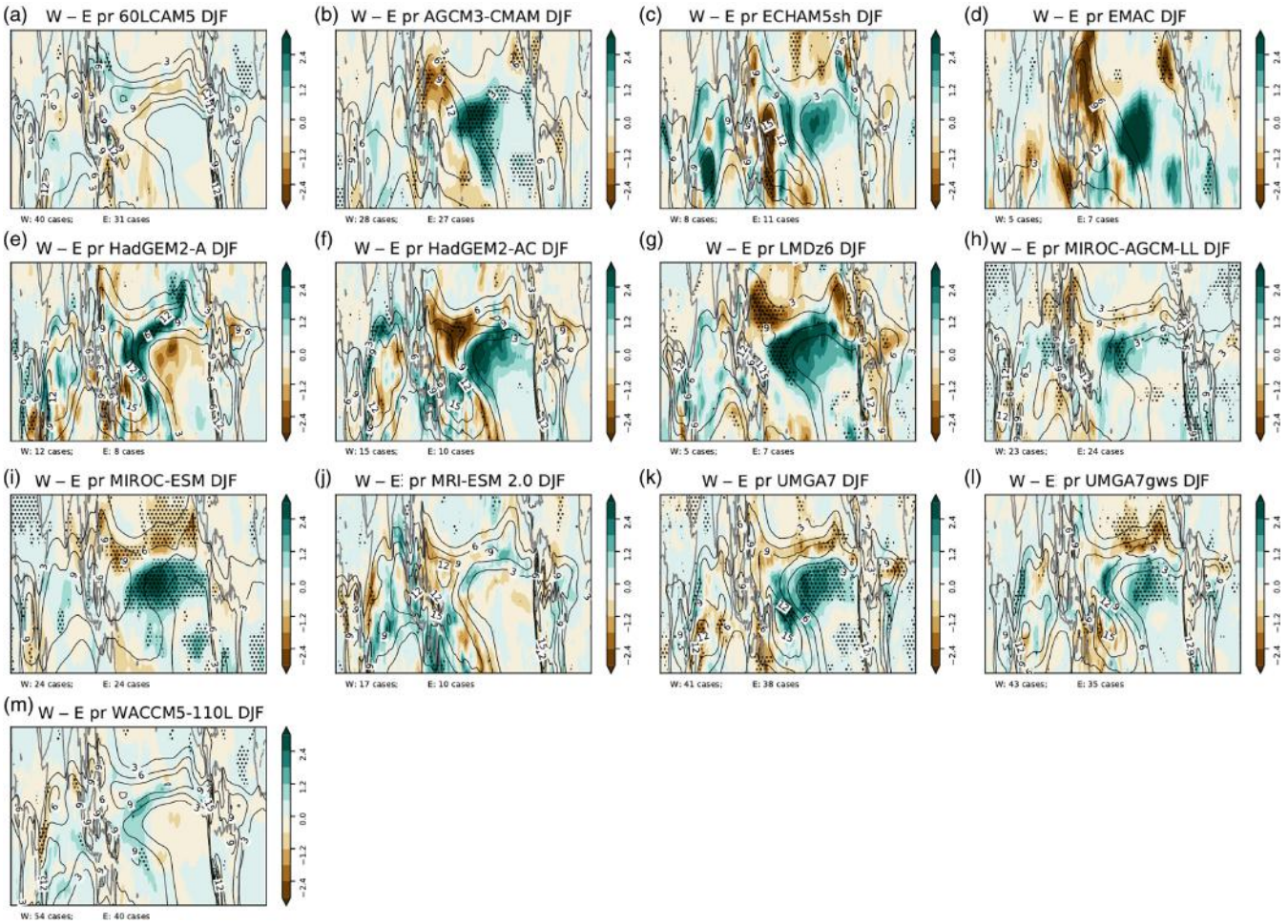

FIGURE 11 The same as Figure 10 but for the Exp1 models in the December–January–February (DJF) season [Colour figure can be viewed at wileyonlinelibrary.com]

monsoon, can be noted in boreal summer. The W – E differences are larger and significant mostly in boreal autumn and winter, markedly over the tropical Pacific Ocean. In the eastern Pacific, the differences are associated with a meridional shift of the ITCZ precipitation band, and longitudinal movement of the South Pacific convergence zone can also be seen. The fact that regions with significant anomalies are quite limited emphasizes how the observed response is highly uncertain.

As the QBO influence on precipitation is larger in boreal winter (Collimore *et al.*, 2003; Klotzbach *et al.*, 2019), we report in Figure 11 the December–January–February mean precipitation and W – E composites for the QBOi models. The intermodel differences in climatological precipitation are major for the seasonal averages, as some models (particularly AGCM3-CMAM, ECHAM5sh, and EMAC) underestimate or even miss the Pacific band of the ITCZ, where the QBO influence is more evident in observations. Conversely, most models overestimate the precipitation over the Maritime Continent. These biases were already documented in previous studies (Horinouchi *et al.*, 2003; Lohmann, 2008; Nam and Quaas, 2012; Watanabe *et al.*, 2011), and by Exp1 design they can only be due to atmospheric processes. Focusing on the W – E differences, as for the tropopause pressures, we find substantial intermodel spread. As expected, models with less realistic average precipitation consequently differ from ERA-Interim results the most. The dry anomalies in the tropical Pacific ITCZ branch and wetting near to the Equator are qualitatively similar to the observed pattern for HadGEM2-AC, LMDz6, MIROC-ESM, UMGA7, and UMGA7gws. The anomalies over the warm pool appear to be less consistent across models. Similar considerations hold for the models during September–October–November (to be compared with Figure 10d), as reported in Supporting information Figure S4. We note that the parametrized NOGW schemes of both LMDz6 and UMGA7gws link the modelled precipitation to the NOGW spectrum properties, but the possible

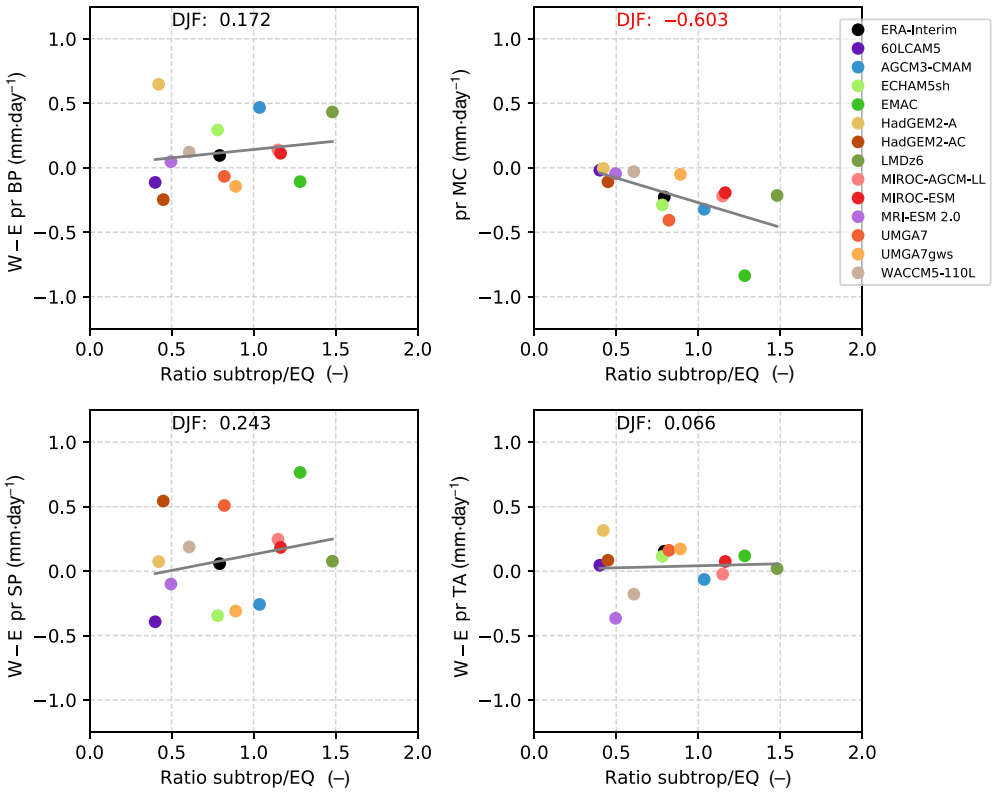

FIGURE 12 The same as Figure 9 but for the precipitation anomalies averaged in four regions (BP, boreal eastern Pacific; MC, Maritime Continent; SP, South Pacific convergence zone, TA: tropical Africa; see text and Supporting information for details). The abscissa is the ratio between the amplitude averaged at subtropical latitudes and that at the Equator. Note that the variable on the abscissa is the same in the four plots [Colour figure can be viewed at wileyonlinelibrary.com]

feedback appears to be small as the tropospheric response for UMGA7 is similar. Compared with the LRT response, the regional patterns for precipitation are more complex. Since robust responses are also found off-Equator, we report in Figure 12 scatter plots of the W − E anomalies against the QBO width averaged over four areas (two already used for the tropopause composites), namely the Maritime Continent, tropical Africa, the South Pacific convergence zone (SP, 5°–20° S, 155° E–150v W) and the boreal eastern Pacific (BP, 2°–12° N, 160° E–90° W). These regions are shown with dashed yellow lines in Figure S5. The QBO width at 70 hPa is estimated as the ratio of the average index amplitude near ±15° divided by that at the Equator, considering three latitudes (in the earlier notation, $(U^{\text{range}}_{+15^\circ} + U^{\text{range}}_{-15^\circ})/2 \cdot U^{\text{range}}_{0^\circ}$). The strength of the relationship depends on the region under consideration, being positive in the two Pacific areas and negative (and significant) over the Maritime Continent. As expected, the intermodel spread is large, also due to the different model precipitation climatologies, but we can see that models with latitudinally wider QBO tend to produce larger W − E anomalies in three out of four regions considered. The correlations are barely significant, since the sign of the anomalies is also not always consistent. No clear relationship can be seen for the tropical African domain, possibly due to the relevance of land–atmosphere coupling, which could overshadow the impact on precipitation from stratospheric processes.

Whereas it is likely that models that have a poor climatological precipitation will not capture the observed QBO response with fidelity, the limited observational record, coupled with the small signal in a field that is highly variable, means that the true response in the real world (and in simulations with a limited ensemble size) is highly uncertain. Until our observational record lengthens, it would be worthwhile focusing on this in a modelling context, with larger ensembles than considered here, so that intermodel differences can be better determined and understood.

4 | CONCLUSIONS

In this work, we analysed the climatological state and variability of the TTL in 13 AGCMs that performed the Exp1 simulations of the QBOi project. All these models internally generate realistic QBOs; therefore, it is possible to study the QBO influence on the TTL, and its connections with the surface, using a multimodel ensemble of free-running simulations.

Temperature biases of both signs near the tropical tropopause are identified in the QBOi multimodel ensemble, leading to water vapour biases in the lower stratosphere. Temperature variability is not only seasonal, but the ENSO, the QBO, and other factors are also important. In a subset of the QBOi models, stratospheric aerosols

due to volcanic eruptions are included, leading to TTL warming in the months following the eruptions. This episodic variability increases the ensemble spread of the climatological water vapour concentrations in the lower stratosphere.

Westerly and easterly QBO phases are associated, by thermal wind balance, with warm and cold anomalies, respectively, in the equatorial lower stratosphere, and induced circulations produce compensating anomalies in the Subtropics. The QBOs of the Exp1 models are generally weaker in the lower stratosphere, and their maximum amplitude is shifted upwards, and latitudinally narrower compared with observations (Bushell *et al.*, 2020). Consistent with small QBO amplitudes and weaker residual circulations, the QBO-induced temperature anomalies at the Equator are realistic but smaller in the QBOi models than in the ERA-Interim reanalysis, and they do not extend as far toward the subtropical lower stratosphere in most models. The strength of the W – E thermal anomalies is correlated with the magnitude of the zonal wind and residual circulation differences, both underestimated by most QBOi models. It should be noted that climatological temperatures differ between the models and QBO-related anomalies are difficult to isolate, due to their fine-scale structures and relative phasing of zonal wind variability and induced responses.

Further analyses have been dedicated to the modelled QBO impact on the tropopause pressure and tropical precipitation. Observational studies indicate that the lower stratospheric QBO has a discernible influence on these variables, besides other climate modes of variability such as ENSO (Christiansen *et al.*, 2016; Serva *et al.*, 2020). As this connection is more robust during the boreal winter season, further studies should investigate the alignment between tropospheric and QBO seasonality. The small amplitude in the lower stratosphere of the simulated QBOs may explain why their influence is generally underestimated by QBOi models year-round.

Tropopause pressure changes in QBOi models are generally smaller than those obtained for the reanalysis, and precipitation anomalies are weaker or in some cases reversed (even if the uncertainty of the observed response is also large, complicating the assessment of the models). The simulated QBO influence is more evident during boreal winter, as in observations. For precipitation, biases in the simulation of the ITCZ structure are associated with substantial differences in patterns for some models. In particular, the eastern tropical Pacific ITCZ is not realistically simulated, and the anomalies associated with the QBO are of the opposite sign from those observed in some cases. The latitudinal extent of the QBO is found to be only weakly correlated with the realism of the tropical W – E precipitation differences, likely due to the large spread between the precipitation climatologies of the models. However, some models able to reproduce QBO-induced changes at the tropopause (such as UMGA7gws) also simulate realistic responses in precipitation, in the same regions where ENSO effects are more marked. Changes in convective activity due to the QBO are of particular interest, since they may contribute to its teleconnection with the boreal stratosphere (Yamazaki *et al.*, 2020). Interestingly, in some models the NOGW drag properties are linked with total precipitation or parameters of the cumulus scheme. Targeted simulations, like initialized experiments with different surface (Sun *et al.*, 2019) or QBO (Hansen *et al.*, 2013) perturbations, should be performed to determine the eventual sensitivity to the cumulus–QBO coupling.

Nevertheless, we emphasize that the mechanisms connecting the QBO and tropospheric climate variability remain uncertain, and the short observational record does not allow us to firmly establish the details of the interaction. Using larger model ensembles than those considered here would allow us to better quantify the limitations in representing the processes and intermodel differences.

To summarize, the model biases that affect the simulation of the QBO appear to alter its influence on other climate phenomena. Most QBOi models simulate a temperature response in the lower equatorial and subtropical stratosphere weaker than that observed; and similarly, modulations of the tropopause pressure and tropical precipitation are generally underestimated or not realistic. It is difficult to ascribe these shortcomings to a single aspect of the model formulations, such as the horizontal and vertical resolution, or their cumulus or NOGW parametrizations. In particular, the formulation of cumulus schemes is likely key for representing the effects of vertical wind shear and stability changes due to the QBO on tropical precipitation regimes. To overcome the uncertainty due to sampling variability, longer simulation and larger ensembles would be helpful to better understand the QBO connection with the tropical TTL. Still, a few of the QBOi models are able to reproduce the observed influences, suggesting that basic physical mechanisms can be realistically captured. This implies that skilful prediction of the modulation of tropical rainfall could be achieved with such models, with implications for dynamical forecasting at the subseasonal and seasonal ranges (Scaife *et al.*, 2017).

ACKNOWLEDGEMENTS

We acknowledge with gratitude the modelling groups who contributed their time and effort in creating the Stratosphere–troposphere Processes And their Role in

Climate (SPARC) QBOi Phase-1 multimodel ensemble dataset as described in Butchart *et al.* (2018), for which underpinning support from the WCRP SPARC QBOi activity and SPARC Office is also gratefully acknowledged.

The QBOi data archive was kindly hosted by the Centre for Environmental Data Analysis (CEDA), UK, and processing was performed on the JASMIN infrastructure. The ECMWF is acknowledged for producing and distributing the ERA-Interim reanalysis, downloaded from https://apps.ecmwf.int/datasets/ (last accessed: November 2020). Acknowledgement is made for the use of ECMWF's computing and archive facilities under Special Project SPITSERV. The AOD data can be downloaded from https://data.giss.nasa.gov/modelforce/strataer/ (last accessed: December 2020), and the daily solar flux data are available at https://lasp.colorado.edu/lisird/data/penticton_radio_flux/ (last accessed: December 2020).

FS was supported by the Copernicus Climate Change Service, funded by the EU and implemented by ECMWF. NB was supported by the Met Office Hadley Centre Climate Programme funded by BEIS and Defra. LJG and SO acknowledge funding from the UK Natural Environment Research Council (NERC) through the National Centre for Atmospheric Science (NCAS) ACSIS project (NE/N018001/1) and the NERC Belmont-Forum grant GOTHAM (NE/P006779/1). YK was supported by Japan Society for Promotion of Science (JSPS) KAKENHI (grant nos. JP18H01286, JP19H05702, and JP20H01973) and by the Environment Research and Technology Development Fund (JPMEERF20192004) of the Environmental Restoration and Conservation Agency of Japan. IRS and JHR were supported by the National Center for Atmospheric Research, which is a major facility sponsored by the National Science Foundation under the Cooperative Agreement 1852977. Portions of this study were supported by the Regional and Global Model Analysis (RGMA) component of the Earth and Environmental System Modeling Program of the U.S. Department of Energy's Office of Biological & Environmental Research (BER) via National Science Foundation IA 1844590.

We thank two anonymous reviewers for their useful comments and suggestions that helped us improve the article.

AUTHOR CONTRIBUTIONS

F. Serva: conceptualization; data curation; formal analysis; methodology; writing – original draft; writing – review and editing. **J. A. Anstey:** conceptualization; methodology; writing – original draft; writing – review and editing. **A. C. Bushell:** conceptualization; methodology; writing – original draft; writing – review and editing. **N. Butchart:** conceptualization; methodology; writing – original draft; writing – review and editing. **C. Cagnazzo:** conceptualization; methodology; writing – original draft; writing – review and editing. **L. J. Gray:** conceptualization; methodology; writing – original draft; writing – review and editing. **Y. Kawatani:** conceptualization; methodology; writing – original draft; writing – review and editing. **S. M. Osprey:** conceptualization; methodology; writing – original draft; writing – review and editing. **J. H. Richter:** conceptualization; methodology; writing – original draft; writing – review and editing. **I. R. Simpson:** conceptualization; methodology; writing – original draft; writing – review and editing.

CONFLICT OF INTEREST

The authors declare no conflict of interest.

ORCID

F. Serva https://orcid.org/0000-0002-7118-0817
J. A. Anstey https://orcid.org/0000-0001-6366-8647
A. C. Bushell https://orcid.org/0000-0001-5683-4387
S. M. Osprey https://orcid.org/0000-0002-8751-1211
J. H. Richter https://orcid.org/0000-0001-7048-0781

REFERENCES

Abalos, M., Randel, W.J. and Serrano, E. (2012) Variability in upwelling across the tropical tropopause and correlations with tracers in the lower stratosphere. *Atmospheric Chemistry and Physics*, 12(23), 11505–11517.

Andrews, D.G., Holton, J.R. and Leovy, C.B. (1987) *Middle atmosphere dynamics*. San Diego, CA: Academic Press.

Angell, J.K. (1997) Estimated impact of Agung, El Chichón and Pinatubo volcanic eruptions on global and regional total ozone after adjustment for the QBO. *Geophysical Research Letters*, 24(6), 647–650.

Anstey, J.A., Butchart, N., Hamilton, K. and Osprey, S.M. (2020) The SPARC Quasi-Biennial Oscillation initiative. *Quarterly Journal of the Royal Meteorological Society*, 1–4. https://doi.org/10.1002/qj.3820.

Anstey, J.A., Simpson, I.R., Richter, J.H., Naoe, H., Taguchi, M., Serva, F., Gray, L.J., Butchart, N., Hamilton, K., Osprey, S.M., Bellprat, O., Braesicke, P., Bushell, A.C., Cagnazzo, C., Chen, C.-C., Chun, H.-Y., Garcia, R.R., Holt, L., Kawatani, Y., Kerzenmacher, T., Kim, Y.-H., Lott, F., McLandress, C., Scinocca, J., Stockdale, T.N., Versick, S., Watanabe, S., Yoshida, K. and Yukimoto, S. (2021) Teleconnections of the quasi-biennial oscillation in a multi-model ensemble of QBO-resolving models. *Quarterly Journal of the Royal Meteorological Society*, 1–26. https://doi.org/10.1002/qj.4048.

Baldwin, M.P., Gray, L.J., Dunkerton, T.J., Hamilton, K., Haynes, P.H., Randel, W.J., Holton, J.R., Alexander, M.J., Hirota, I., Horinouchi, T., Jones, D.B.A., Kinnersley, J.S., Marquardt, C., Sato, K. and Takahashi, M. (2001) The quasi-biennial oscillation. *Reviews of Geophysics*, 39(2), 179–229.

Bushell, A.C., Anstey, J.A., Butchart, N., Kawatani, Y., Osprey, S.M., Richter, J.H., Serva, F., Braesicke, P., Cagnazzo, C., Chen, C.-C.,

Chun, H.-Y., Garcia, R.R., Gray, L.J., Hamilton, K., Kerzenmacher, T., Kim, Y.-H., Lott, F., McLandress, C., Naoe, H., Scinocca, J., Smith, A.K., Stockdale, T.N., Versick, S., Watanabe, S., Yoshida, K. and Yukimoto, S. (2020) Evaluation of the quasi-biennial oscillation in global climate models for the SPARC QBO-initiative. *Quarterly Journal of the Royal Meteorological Society*. https://doi.org/10.1002/qj.3765.

Bushell, A.C., Butchart, N., Derbyshire, S.H., Jackson, D.R., Shutts, G.J., Vosper, S.B. and Webster, S. (2015) Parameterized gravity wave momentum fluxes from sources related to convection and large-scale precipitation processes in a global atmosphere model. *Journal of the Atmospheric Sciences*, 72(11), 4349–4371.

Butchart, N., Anstey, J.A., Hamilton, K., Osprey, S., McLandress, C., Bushell, A.C., Kawatani, Y., Kim, Y.-H., Lott, F., Scinocca, J., Stockdale, T.N., Andrews, M., Bellprat, O., Braesicke, P., Cagnazzo, C., Chen, C.-C., Chun, H.-Y., Dobrynin, M., Garcia, R.R., Garcia-Serrano, J., Gray, L.J., Holt, L., Kerzenmacher, T., Naoe, H., Pohlmann, H., Richter, J.H., Scaife, A.A., Schenzinger, V., Serva, F., Versick, S., Watanabe, S., Yoshida, K. and Yukimoto, S. (2018) Overview of experiment design and comparison of models participating in phase 1 of the SPARC Quasi-Biennial Oscillation initiative (QBOi). *Geoscientific Model Development*, 11(3), 1009–1032.

Butchart, N., Scaife, A.A., Austin, J., Hare, S.H.E. and Knight, J.R. (2003) Quasi-biennial oscillation in ozone in a coupled chemistry–climate model. *Journal of Geophysical Research: Atmospheres*, 108(D15), 4486.

Choi, H.-J. and Chun, H.-Y. (2011) Momentum flux spectrum of convective gravity waves. Part I: An update of a parameterization using mesoscale simulations. *Journal of the Atmospheric Sciences*, 68, 739–759.

Christiansen, B., Yang, S. and Madsen, M.S. (2016) Do strong warm ENSO events control the phase of the stratospheric QBO?. *Geophysical Research Letters*, 43(19), 10489–10495. https://doi.org/10.1002/2016GL070751.

Collimore, C.C., Martin, D.W., Hitchman, M.H., Huesmann, A. and Waliser, D.E. (2003) On the relationship between the QBO and tropical deep convection. *Journal of Climate*, 16(15), 2552–2568.

Dai, A. (2006) Precipitation characteristics in eighteen coupled climate models. *Journal of Climate*, 19(18), 4605–4630.

Davis, C.A., Ahijevych, D.A., Haggerty, J.A. and Mahoney, M.J. (2014) Observations of temperature in the upper troposphere and lower stratosphere of tropical weather disturbances. *Journal of the Atmospheric Sciences*, 71(5), 1593–1608.

Dee, D.P., Uppala, S.M., Simmons, A.J., Berrisford, P., Poli, P., Kobayashi, S., Andrae, U., Balmaseda, M.A., Balsamo, G., Bauer, P., Bechtold, P., Beljaars, A.C.M., van de Berg, L., Bidlot, J., Bormann, N., Delsol, C., Dragani, R., Fuentes, M., Geer, A.J., Haimberger, L., Healy, S.B., Hersbach, H., Hólm, E.V., Isaksen, L., Kållberg, P., Köhler, M., Matricardi, M., McNally, A.P., Monge-Sanz, B.M., Morcrette, J.-J., Park, B.-K., Peubey, C., de Rosnay, P., Tavolato, C., Thépaut, J.-N. and Vitart, F. (2011) The ERA-Interim reanalysis: Configuration and performance of the data assimilation system. *Quarterly Journal of the Royal Meteorological Society*, 137(656), 553–597.

de la Cámara, A. and Lott, F. (2015) A parameterization of gravity waves emitted by fronts and jets. *Geophysical Research Letters*, 42, 2071–2078.

Emori, S., Nozawa, T., Numaguti, A. and Uno, I. (2001) Importance of cumulus parameterization for precipitation simulation over east Asia in June. *Journal of the Meteorological Society of Japan*, 79(4), 939–947.

Fasullo, J.T., Otto-Bliesner, B.L. and Stevenson, S. (2018) ENSO's changing influence on temperature, precipitation, and wildfire in a warming climate. *Geophysical Research Letters*, 45(17), 9216–9225.

Fueglistaler, S., Dessler, A.E., Dunkerton, T.J., Folkins, I., Fu, Q. and Mote, P.W. (2009) Tropical tropopause layer. *Reviews of Geophysics*, 47(1), RG1004.

Fujiwara, M., Hibino, T., Mehta, S.K., Gray, L., Mitchell, D. and Anstey, J. (2015) Global temperature response to the major volcanic eruptions in multiple reanalysis data sets. *Atmospheric Chemistry and Physics*, 15, 13507–13518.

Fujiwara, M., Suzuki, J., Gettelman, A., Hegglin, M.I., Akiyoshi, H. and Shibata, K. (2012) Wave activity in the tropical tropopause layer in seven reanalysis and four chemistry climate model data sets. *Journal of Geophysical Research: Atmospheres*, 117(D12), D12105.

Garfinkel, C.I. and Hartmann, D.L. (2011) The influence of the quasi-biennial oscillation on the troposphere in winter in a hierarchy of models. Part I: Simplified dry GCMs. *Journal of the Atmospheric Sciences*, 68(6), 1273–1289.

Gettelman, A., Hegglin, M.I., Son, S.-W., Kim, J., Fujiwara, M., Birner, T., Kremser, S., Rex, M., Añel, J.A., Akiyoshi, H., Austin, J., Bekki, S., Braesicke, P., Brühl, C., Butchart, N., Chipperfield, M., Dameris, M., Dhomse, S., Garny, H., Hardiman, S.C., Jöckel, P., Kinnison, D.E., Lamarque, J.F., Mancini, E., Marchand, M., Michou, M., Morgenstern, O., Pawson, S., Pitari, G., Plummer, D., Pyle, J.A., Rozanov, E., Scinocca, J., Shepherd, T.G., Shibata, K., Smale, D., Teyssèdre, H. and Tian, W. (2010) Multimodel assessment of the upper troposphere and lower stratosphere: Tropics and global trends. *Journal of Geophysical Research: Atmospheres*, 115(D3), D00M08.

Giorgetta, M.A. and Bengtsson, L. (1999) Potential role of the quasi-biennial oscillation in the circulation model experiments. *Journal of Geophysical Research: Atmospheres*, 104(D6), 6003–6019.

Giorgetta, M.A., Manzini, E. and Roeckner, E. (2002) Forcing of the quasi-biennial oscillation from a broad spectrum of atmospheric waves. *Geophysical Research Letters*, 29(8), 86–1–86-4.

Gray, L.J., Anstey, J.A., Kawatani, Y., Lu, H., Osprey, S. and Schenzinger, V. (2018) Surface impacts of the quasi biennial oscillation. *Atmospheric Chemistry and Physics*, 18(11), 8227–8247.

Gray, L.J., Beer, J., Geller, M., Haigh, J.D., Lockwood, M., Matthes, K., Cubasch, U., Fleitmann, D., Harrison, G., Hood, L., Luterbacher, J., Meehl, G.A., Shindell, D., van Geel, B. and White, W. (2010) Solar influences on climate. *Reviews of Geophysics*, 48(4), RG4001.

Gregory, D. and Rowntree, P.R. (1990) A mass flux convection scheme with representation of cloud ensemble characteristics and stability-dependent closure. *Monthly Weather Review*, 118(7), 1483–1506.

Hansen, F., Matthes, K. and Gray, L.J. (2013) Sensitivity of stratospheric dynamics and chemistry to QBO nudging width in the chemistry—Climate model WACCM. *Journal of Geophysical Research: Atmospheres*, 118(18), 10464–10474.

Hansen, J.M., Sato, R., Ruedy, A., Lacis, K., Asamoah, S., Borenstein, E., Brown, B., Cairns, G., Caliri, M., Campbell, B., Curran, S., de Castro, L., Druyan, M., Fox, C., Johnson, J., Lerner, M.,

McCormick, R., Miller, P., Minnis, A., Morrison, L., Pandolfo, I., Ramberran, F., Zaucker, M., Robinson, P., Russell, K., Shah, P., Stone, I., Tegen, L., Thomason, J., Wilder and Wilson, H. (1996). A Pinatubo climate modeling investigation. In G. Fiocco, D. Fuà, and G. Visconti (Eds.), *The Mount Pinatubo eruption: Effects on the atmosphere and climate*, NATO ASI Series (Vol. 42 pp. 233–272). Berlin, Germany: Springer-Verlag.

Hardiman, S.C., Boutle, I.A., Bushell, A.C., Butchart, N., Cullen, M.J.P., Field, P.R., Furtado, K., Manners, J.C., Milton, S.F., Morcrette, C., O'Connor, F.M., Shipway, B.J., Smith, C., Walters, D.N., Willett, M.R., Williams, K.D., Wood, N., Abraham, N.L., Keeble, J., Maycock, A.C., Thuburn, J. and Woodhouse, M.T. (2015) Processes controlling tropical tropopause temperature and stratospheric water vapor in climate models. *Journal of Climate*, 28(16), 6516–6535.

Hatsushika, H. and Yamazaki, K. (2001) Interannual variations of temperature and vertical motion at the tropical tropopause associated with ENSO. *Geophysical Research Letters*, 28(15), 2891–2894.

Hines, C.O. (1997) Doppler-spread parameterization of gravity-wave momentum deposition in the middle atmosphere. Part 2: Broad and quasi monochromatic spectra, and implementation. *Journal of Atmospheric and Solar-Terrestrial Physics*, 59(4), 387–400.

Holt, L.A., Lott, F., Garcia, R.R., Kiladis, G.N., Cheng, Y.-M., Anstey, J.A., Braesicke, P., Bushell, A.C., Butchart, N., Cagnazzo, C., Chen, C.-C., Chun, H.-Y., Kawatani, Y., Kerzenmacher, T., Kim, Y.-H., McLandress, C., Naoe, H., Osprey, S., Richter, J.H., Scaife, A.A., Scinocca, J., Serva, F., Versick, S., Watanabe, S., Yoshida, K. and Yukimoto, S. (2020) An evaluation of tropical waves and wave forcing of the QBO in the QBOi models. *Quarterly Journal of the Royal Meteorological Society*. https://doi.org/10.1002/qj.3827.

Horinouchi, T., Pawson, S., Shibata, K., Langematz, U., Manzini, E., Giorgetta, M.A., Sassi, F., Wilson, R.J., Hamilton, K., de Grandpré, J. and Scaife, A.A. (2003) Tropical cumulus convection and upward-propagating waves in middle-atmospheric GCMs. *Journal of the Atmospheric Sciences*, 60(22), 2765–2782.

Hourdin, F., Grandpeix, J.-Y., Rio, C., Bony, S., Jam, A., Cheruy, F., Rochetin, N., Fairhead, L., Idelkadi, A., Musat, I., Dufresne, J.-L., Lahellec, A., Lefebvre, M.-P. and Roehrig, R. (2013) LMDz5b: The atmospheric component of the IPSL climate model with revisited parameterizations for clouds and convection. *Climate Dynamics*, 40(9), 2193–2222.

Huesmann, A.S. and Hitchman, M.H. (2001) The stratospheric quasi-biennial oscillation in the NCEP reanalyses: Climatological structures. *Journal of Geophysical Research: Atmospheres*, 106(D11), 11859–11874.

Kawatani, Y., Takahashi, M., Sato, K., Alexander, S.P. and Tsuda, T. (2009) Global distribution of atmospheric waves in the equatorial upper troposphere and lower stratosphere: AGCM simulation of sources and propagation. *Journal of Geophysical Research: Atmospheres*, 114(D1), D01102.

Kawatani, Y., Watanabe, S., Sato, K., Dunkerton, T.J., Miyahara, S. and Takahashi, M. (2010) The roles of equatorial trapped waves and internal inertia–gravity waves in driving the quasi-biennial oscillation. Part I: Zonal mean wave forcing. *Journal of the Atmospheric Sciences*, 67(4), 963–980.

Klotzbach, P., Abhik, S., Hendon, H.H., Bell, M., Lucas, C., Marshall, G. and Oliver, E.C.J. (2019) On the emerging relationship between the stratospheric quasi-biennial oscillation and the Madden–Julian oscillation. *Scientific Reports*, 9(1), 2981.

Li, D., Shine, K.P. and Gray, L.J. (1995) The role of ozone-induced diabatic heating anomalies in the quasi-biennial oscillation. *Quarterly Journal of the Royal Meteorological Society*, 121(524), 937–943.

Liess, S. and Geller, M.A. (2012) On the relationship between QBO and distribution of tropical deep convection. *Journal of Geophysical Research: Atmospheres*, 117(D3), D03108.

Lindzen, R.S. (1981) Turbulence and stress owing to gravity wave and tidal breakdown. *Journal of Geophysical Research*, 86, 9707–9714.

Löffler, M., Brinkop, S. and Jöckel, P. (2016) Impact of major volcanic eruptions on stratospheric water vapour. *Atmospheric Chemistry and Physics*, 16, 6547–6562.

Lohmann, U. (2008) Global anthropogenic aerosol effects on convective clouds in ECHAM5-HAM. *Atmospheric Chemistry and Physics*, 8, 2115–2131.

Lott, F. and Guez, L. (2013) A stochastic parameterization of the gravity waves due to convection and its impact on the equatorial stratosphere. *Journal of Geophysical Research: Atmospheres*, 118(16), 8897–8909.

Lott, F., Guez, L. and Maury, P. (2012) A stochastic parameterization of non-orographic gravity waves: Formalism and impact on the equatorial stratosphere. *Geophysical Research Letters*, 39, L06807.

Luan, L., Staten, P.W., Ao, C.O. and Fu, Q. (2020) Seasonal and annual changes of the regional tropical belt in GPS-RO measurements and reanalysis datasets. *Journal of Climate*, 33(10), 4083–4094.

Ming, A., Maycock, A.C., Hitchcock, P. and Haynes, P. (2017) The radiative role of ozone and water vapour in the annual temperature cycle in the tropical tropopause layer. *Atmospheric Chemistry and Physics*, 17, 5677–5701.

Mitchell, D.M., Gray, L.J., Fujiwara, M., Hibino, T., Anstey, J.A., Ebisuzaki, W., Harada, Y., Long, C., Misios, S., Stott, P.A. and Tan, D. (2015) Signatures of naturally induced variability in the atmosphere using multiple reanalysis datasets. *Quarterly Journal of the Royal Meteorological Society*, 141(691), 2011–2031.

Nam, C.C.W. and Quaas, J. (2012) Evaluation of clouds and precipitation in the ECHAM5 general circulation model using CALIPSO and CloudSat satellite data. *Journal of Climate*, 25(14), 4975–4992.

Nie, J. and Sobel, A.H. (2015) Responses of tropical deep convection to the QBO: Cloud-resolving simulations. *Journal of the Atmospheric Sciences*, 72(9), 3625–3638.

Nordeng, T.E. (1994) *Extended versions of the convective parametrization scheme at ECMWF and their impact on the mean and transient activity of the model in the Tropics* (ECMWF Technical Report No. 206). Reading, UK: ECMWF. ECMWF Technical Report.

Oh, J., Son, S.-W., Williams, K., Walters, D., Kim, J., Willett, M., Earnshaw, P., Bushell, A., Kim, Y. and Kim, J. (2018) Ozone sensitivity of tropical upper-troposphere and stratosphere temperature in the MetOffice Unified Model. *Quarterly Journal of the Royal Meteorological Society*, 144(715), 2001–2009.

Plumb, R.A. and Bell, R.C. (1982) A model of the quasi-biennial oscillation on an equatorial beta-plane. *Quarterly Journal of the Royal Meteorological Society*, 108, 335–352.

Randel, W.J. and Jensen, E.J. (2013) Physical processes in the tropical tropopause layer and their roles in a changing climate. *Nature Geoscience*, 6(3), 169–176.

Randel, W.J. and Wu, F. (2015) Variability of zonal mean tropical temperatures derived from a decade of GPS radio occultation data. *Journal of the Atmospheric Sciences*, 72, 1261–1275.

Randel, W.J., Wu, F. and Gaffen, D.J. (2000) Interannual variability of the tropical tropopause derived from radiosonde data and NCEP reanalyses. *Journal of Geophysical Research: Atmospheres*, 105(D12), 15509–15523.

Richter, J.H., Anstey, J.A., Butchart, N., Kawatani, Y., Meehl, G.A., Osprey, S. and Simpson, I.R. (2020) Progress in simulating the quasi-biennial oscillation in CMIP models. *Journal of Geophysical Research: Atmospheres*, 125(8), e2019JD032362.

Richter, J.H., Sassi, F. and Garcia, R.R. (2010) Toward a physically based gravity wave source parameterization in a general circulation model. *Journal of the Atmospheric Sciences*, 67(1), 136–156.

Rieckh, T., Scherllin-Pirscher, B., Ladstädter, F. and Foelsche, U. (2014) Characteristics of tropopause parameters as observed with GPS radio occultation. *Atmospheric Measurement Techniques*, 7(11), 3947–3958.

Robock, A. (2004). Climatic impact of volcanic emissions. In R.S.J. Sparks and C.J. Hawkesworth (Eds.), *The state of the planet: Frontiers and challenges in geophysics*, IUGG Geophysical Monograph Series (Vol. 150 pp. 125–134). Washington, DC: American Geophysical Union.

Rosenlof, K.H. (1995) Seasonal cycle of the residual mean meridional circulation in the stratosphere. *Journal of Geophysical Research: Atmospheres*, 100(D3), 5173–5191.

Scaife, A.A., Butchart, N., Warner, C.D., Stainforth, D., Norton, W. and Austin, J. (2000) Realistic quasi-biennial oscillations in a simulation of the global climate. *Geophysical Research Letters*, 27(21), 3481–3484.

Scaife, A.A., Comer, R.E., Dunstone, N.J., Knight, J.R., Smith, D.M., MacLachlan, C., Martin, N., Peterson, K.A., Rowlands, D., Carroll, E.B., Belcher, S. and Slingo, J. (2017) Tropical rainfall, Rossby waves and regional winter climate predictions. *Quarterly Journal of the Royal Meteorological Society*, 143(702), 1–11.

Scinocca, J.F. (2003) An accurate spectral nonorographic gravity wave drag parameterization for general circulation models. *Journal of the Atmospheric Sciences*, 60, 667–682.

Schoeberl, M.R., Jensen, E.J., Pfister, L., Ueyama, R., Avery, M. and Dessler, A.E. (2018) Convective hydration of the upper troposphere and lower stratosphere. *Journal of Geophysical Research: Atmospheres*, 123(9), 4583–4593.

Seidel, D.J., Ross, R.J., Angell, J.K. and Reid, G.C. (2001) Climatological characteristics of the tropical tropopause as revealed by radiosondes. *Journal of Geophysical Research: Atmospheres*, 106(D8), 7857–7878.

Serva, F., Cagnazzo, C., Christiansen, B. and Yang, S. (2020) The influence of ENSO events on the stratospheric QBO in a multi-model ensemble. *Climate Dynamics*, 54(3), 2561–2575.

Serva, F., Cagnazzo, C., Riccio, A. and Manzini, E. (2018) Impact of a stochastic nonorographic gravity wave parameterization on the stratospheric dynamics of a general circulation model. *Journal of Advances in Modeling Earth Systems*, 10(9), 2147–2162.

Soden, B.J., Wetherald, R.T., Stenchikov, G.L. and Robock, A. (2002) Global cooling after the eruption of Mount Pinatubo: A test of climate feedback by water vapor. *Science*, 296(5568), 727–730.

Sun, J., Zhang, K., Wan, H., Ma, P.-L., Tang, Q. and Zhang, S. (2019) Impact of nudging strategy on the climate representativeness and hindcast skill of constrained EAMv1 simulations. *Journal of Advances in Modeling Earth Systems*, 11(12), 3911–3933.

Takahashi, M. (1996) Simulation of the stratospheric quasi-biennial oscillation using a general circulation model. *Geophysical Research Letters*, 23(6), 661–664.

Tapping, K.F. (2013) The 10.7 cm solar radio flux (F10.7). *Space Weather*, 11(7), 394–406.

Tegtmeier, S., Anstey, J., Davis, S., Dragani, R., Harada, Y., Ivanciu, I., Pilch Kedzierski, R., Krüger, K., Legras, B., Long, C., Wang, J.S., Wargan, K. and Wright, J.S. (2020) Temperature and tropopause characteristics from reanalyses data in the tropical tropopause layer. *Atmospheric Chemistry and Physics*, 20(2), 753–770.

Tegtmeier, S., Anstey, J., Davis, S., Ivanciu, I., Jia, Y., McPhee, D. and Pilch Kedzierski, R. (2020a) Zonal asymmetry of the QBO temperature signal in the tropical tropopause region. *Geophysical Research Letters*, 47, e2020GL089533.

Tian, E.W., Su, H., Tian, B. and Jiang, J.H. (2019) Interannual variations of water vapor in the tropical upper troposphere and the lower and middle stratosphere and their connections to ENSO and QBO. *Atmospheric Chemistry and Physics*, 19(15), 9913–9926.

Tiedtke, M. (1989) A comprehensive mass flux scheme for cumulus parameterization in large-scale models. *Monthly Weather Review*, 117(8), 1779–1800.

Toohey, M., Krüger, K., Bittner, M., Timmreck, C. and Schmidt, H. (2014) The impact of volcanic aerosol on the Northern Hemisphere stratospheric polar vortex: Mechanisms and sensitivity to forcing structure. *Atmospheric Chemistry and Physics*, 14(23), 13063–13079.

Wang, T., Zhang, Q., Hannachi, A., Hirooka, T. and Hegglin, M.I. (2020) Tropical water vapour in the lower stratosphere and its relationship to tropical/extratropical dynamical processes in ERA5. *Quarterly Journal of the Royal Meteorological Society*, 146(730), 2432–2449.

Warner, C.D. and McIntyre, M.E. (1999) Toward an ultra-simple spectral gravity wave parameterization for general circulation models. *Earth, Planets and Space*, 51, 475–484.

Watanabe, S., Hajima, T., Sudo, K., Nagashima, T., Takemura, T., Okajima, H., Nozawa, T., Kawase, H., Abe, M., Yokohata, T., Ise, T., Sato, H., Kato, E., Takata, K., Emori, S. and Kawamiya, M. (2011) MIROC-ESM 2010: Model description and basic results of CMIP5-20c3m experiments. *Geoscientific Model Development*, 4(4), 845–872.

Xian, T. and Fu, Y. (2015) Characteristics of tropopause-penetrating convection determined by TRMM and COSMIC GPS radio occultation measurements. *Journal of Geophysical Research: Atmospheres*, 120(14), 7006–7024.

Yamazaki, K., Nakamura, T., Ukita, J. and Hoshi, K. (2020) A tropospheric pathway of the stratospheric quasi-biennial oscillation (QBO) impact on the boreal winter polar vortex. *Atmospheric Chemistry and Physics*, 20(8), 5111–5127.

Yoshimura, H., Mizuta, R. and Murakami, H. (2015) A spectral cumulus parameterization scheme interpolating between two convective updrafts with semi-Lagrangian calculation of transport by compensatory subsidence. *Monthly Weather Review*, 143(2), 597–621.

Yukimoto, S., Kawai, H., Koshiro, T., Oshima, N., Yoshida, K., Urakawa, S., Tsujino, H., Deushi, M., Tanaka, T., Hosaka, M., Yabu, S., Yoshimura, H., Shindo, E., Mizuta, R., Obata, A.,

Adachi, Y. and Ishii, M. (2019) The Meteorological Research Institute Earth System Model version 2.0, MRI-ESM2.0: Description and basic evaluation of the physical component. *Journal of the Meteorological Society of Japan*, 97(5), 931–965.

Zhang, G. and McFarlane, N.A. (1995) Sensitivity of climate simulations to the parameterization of cumulus convection in the Canadian Climate Centre general circulation model. *Atmosphere–Ocean*, 33(3), 407–446.

SUPPORTING INFORMATION

Additional supporting information may be found online in the Supporting Information section at the end of this article.

How to cite this article: Serva, F., Anstey, J.A., Bushell, A.C., Butchart, N., Cagnazzo, C., Gray, L.J. *et al*. (2022) The impact of the QBO on the region of the tropical tropopause in QBOi models: Present-day simulations. *Quarterly Journal of the Royal Meteorological Society*, 148(745), 1945–1964. Available from: https://doi.org/10.1002/qj.4287